Marine and Petroleum Geology 96 (2018) 348–370

Contents lists available at ScienceDirect

Marine and Petroleum Geology

journal homepage: www.elsevier.com/locate/marpetgeo

Research paper

Mechanical compaction in chlorite-coated sandstone reservoirs – Examples from Middle – Late Triassic channels in the southwestern Barents Sea

Lina Hedvig Line[a,*], Jens Jahren[a], Helge Hellevang[a,b]

[a] Department of Geosciences, University of Oslo, P.O. Box 1047, Blindern, 0316 Oslo, Norway
[b] The University Centre in Svalbard (UNIS), Pb. 156, 9171 Longyearbyen, Norway

ARTICLE INFO

Keywords:
Barents sea
Triassic
Diagenesis
Reservoir quality
Chlorite coating

ABSTRACT

The relationship between diagenetic evolution and reservoir quality in large-scale Middle – Late Triassic aged channel systems (up to 20 km wide) in the southwestern Barents Sea is investigated through core plug data, XRD, SEM- and modal analyses. The studied channel systems are likely sourced from the southeastern Uralide mountain range and are characterized by chemically unstable clastic sediment and well-developed, porosity-preserving chlorite coatings. Chlorite coatings occupy potential quartz nucleation sites on the framework grain surfaces and likely prevent significant chemical compaction in deeply buried sandstones. Porosity-reduction is believed to follow mechanical compaction trends of similar sandstone compositions. Modelling and prediction of porosity preservation in Middle - Late Triassic channel sandstones in the study area is therefore possible, if temperature histories and sandstone compositions are well constrained.

The tidally influenced channel and fluvial-dominated channels in this study show significant variation in reservoir quality. These differences are found to be linked to amount of allogenic matrix and grain size, which significantly reduces the permeability in the tidally influenced channel. If seismic distinction between different channel types is impossible, the distribution of permeability is considered unpredictable.

Chlorite coatings in the investigated channels are interpreted to be diagenetic overprints of a precursor clay phase, which appears to have a strong link to the Uralian provenance. Coating precursor emplacement likely occurs prior to significant burial, but the exact physical conditions enabling this process remain elusive without systematic laboratory and analogue studies.

1. Introduction

Chlorite coatings are responsible for preserving anomalously high porosities in deeply buried Middle – Late Triassic sandstone reservoirs in the structurally complex southwestern Barents Sea. Efficient inhibition of quartz nucleation on detrital grain surfaces retard the onset of significant chemical compaction, making these sandstones a unique natural laboratory for studying mechanical compaction in siliciclastic sandstones at various burial depths.

Channel sandstone systems sourced from the Uralian Orogeny have been the subject of intense petroleum exploration and research campaigns in the southwestern Barents Sea during recent years, with a well-defined sequence stratigraphic framework being established (Glørstad-Clark et al., 2010, 2011; Klausen et al., 2014, 2015; Eide et al., 2017; Haile et al., 2017). Despite optimistic predictions from Norwegian state authorities (Directorate, 2016), recent exploration well results have proven disappointing due to key risk factors such as reservoir quality, hydrocarbon charge and migration and seal capacity. Differential uplift and chemically unstable sandstone composition challenge the established prediction methods. Increasing the ability to predict the presence of high-quality reservoirs units prior to drilling has great economic potential. Chlorite coating development has been described in multiple publications from laboratory studies (Matlack et al., 1989; Aagaard et al., 2000; Haile et al., 2015) and natural sandstones all over the world (Ryan and Reynolds, 1996; Billault et al., 2003; Gould et al., 2010; Dowey et al., 2012), but few published studies describe chlorite coatings in Triassic channels in the southwestern Barents Sea in detail (Haile et al., 2017).

This paper investigates the diagenetic evolution and reservoir quality of Middle – Late Triassic channel sandstones of the Kobbe and Snadd formations (Fig. 1b), and evaluates the predictability of high-quality sandstone reservoirs within the Triassic petroleum play in the southwestern Barents Sea. The origin, distribution and emplacement of chlorite coatings are also discussed. Results from this study may provide useful input for modelling of compaction in chlorite-coated sandstones with chemically unstable compositions.

* Corresponding author.
E-mail address: l.h.line@geo.uio.no (L.H. Line).

https://doi.org/10.1016/j.marpetgeo.2018.05.025
Received 13 April 2018; Accepted 28 May 2018
Available online 01 June 2018

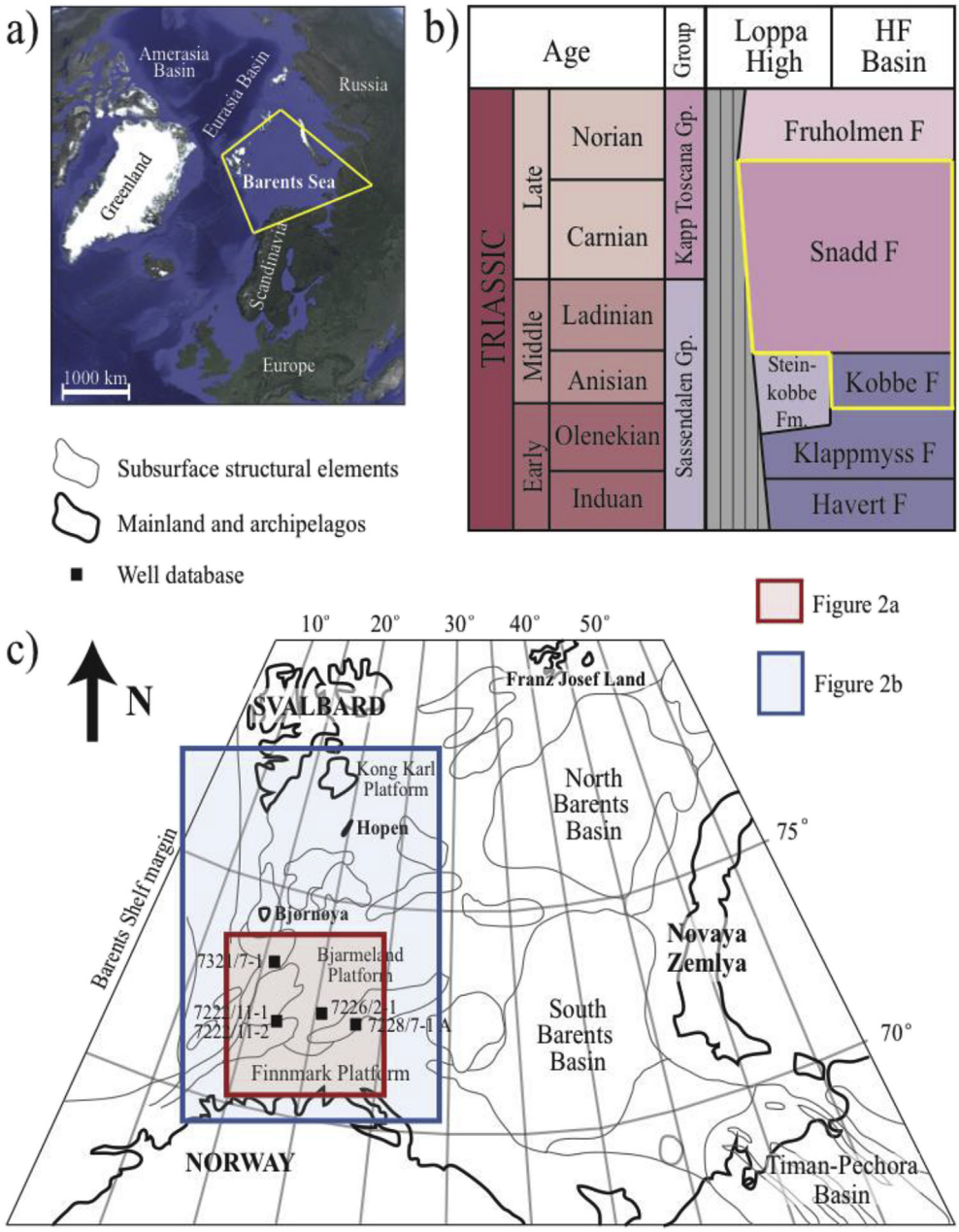

Fig. 1. a) The greater Barents Sea region (yellow frame) covers an area of approximately 1.3 million km^2 (figure modified Google Earth, 2016). b) Simple stratigraphic chart of the Triassic period in the southwestern Barents Sea, modified after Mørk et al. (1999). Cored sections used in this study cover the Anisian Kobbe and the Carnian Snadd formations, indicated in yellow frame. c) The well database is located in the southwestern part of the Norwegian Barents Shelf. Figure modified from NPD Factpages and Worsley (2008). Red and blue frames indicate the position of Fig. 2a and b. (For interpretation of the references to color in this figure legend, the reader is referred to the Web version of this article.)

2. Geological background

The Norwegian sector of the Barents Sea includes the area bordered by the Norwegian mainland to the south, the deep Atlantic Ocean margin to the west, the Svalbard archipelago to the north and the Norwegian-Russian maritime delimitation line as its eastern boundary (Fig. 1c). In contrast to the large and deep sag basins characterizing the eastern Russian sector, the western Norwegian Barents Sea region is characterized by a complex mosaic of structural highs, platforms and basins bound to the west by a continental margin (Fig. 1b). The present basin configuration is the result of two major tectonic phases post-dating the compressional movements that prevailed during the Caledonian Orogeny, and subsequent rescission and erosion (Henriksen et al., 2011).

During Late Devonian to mid-Permian, intra-cratonic rifting resulted in the development of deep basins, such as the Nordkapp and Sverdrup Basins, along weakened crustal sutures inherited from the Caledonian Orogeny. The latitudinal position of the Barents Shelf at the time facilitated arid conditions, and the deep basins were filled by thick evaporate and carbonate deposits. The shelf experienced regional subsidence and increased clastic sedimentation during the Middle Permian, as a response to the Uralide hinterland development in the east (Ronnevik et al., 1982).

Decreasing subsidence rates and cessation of major tectonic events characterize the Triassic period, and post-Permian transgression created accommodation space on the shelf (Lundschien et al., 2014). Several sequences of major deltaic progradations towards northwest filled the basin during the Triassic and Early Jurassic, where sediments deposited on the southwestern Barents Shelf likely originated from the southern Caledonian and southeastern Uralian provenance regions (Glørstad-Clark et al., 2010, 2011; Høy and Lundschien, 2011; Anell et al., 2014; Bue and Andresen, 2014; Klausen et al., 2015; Eide et al., 2017).

The distribution of high-quality Triassic sandstone reservoirs, typically bearing a Caledonian provenance signature, appears to be restricted to the southern Hammerfest Basin and the Finnmark Platform margins (Fleming et al., 2016). Remaining areas on the southwestern

Barents Shelf are dominated by Triassic sediments with a Uralian signature (Bergan and Knarud, 1993; Mørk, 1999; Fleming et al., 2016; Haile et al., 2017). Extensional tectonism during the mid- Late Jurassic generated deep, anoxic basins along the present-day Norwegian continental shelf, which facilitated deposition of organic-rich source rocks from the southern North Sea Basin to the Barents Sea Basin in the north. This Kimmeridgian rifting eventually led to the development of the Euramerican Basin at the northern margins of the Barents Shelf, accompanied by widespread magmatism and uplift of the northern flank. The opening of the Norwegian-Greenland Sea led firstly to uplift and erosion throughout the Late Cretaceous, which was followed by a transpressional and subsequent transtensional regime across the shelf during the Cenozoic (Worsley, 2008; Henriksen et al., 2011).

Cenozoic strata are absent on platform areas (e.g. Finnmark and Bjarmeland Platforms), at parts of the Loppa High and generally in the northeastern regions of the Barents Sea. Truncated Cretaceous strata below Quaternary sediments indicate a significant regional erosional hiatus, likely associated with the opening of the Norwegian-Greenland Sea and post-uplift glaciations in Late Pliocene-Pleistocene. Rocks in the uplifted regions are currently not at their maximum burial depths (Henriksen et al., 2011; Baig et al., 2016), and the net erosion in the southwestern Barents Sea has been estimated to range from 0.7 to 3.5 km, with significant local variations within the basin (Cavanagh et al., 2006). An overall increase in net erosion magnitude towards east and northeast is observed (Baig et al., 2016). The estimated geothermal gradients of the southwestern Barents Sea, calculated based on present-day bottom hole temperatures (BHT) and drilling stem tests (DST) are 31 °C and 38 °C, respectively (Smelror et al., 2009).

For a thorough review of the tectonic history of the Barents Shelf, the reader is referred to Rønnevik et al. (1982), Faleide et al. (1984), Gabrielsen et al. (1990), Gudlaugsson et al. (1998) and recent revision studies by Worsley (2008), Glørstad-Clark et al. (2010), Glørstad-Clark et al. (2011), Høy and Lundschien (2011) and Henriksen et al. (2011).

2.1. Anisian sedimentation - Kobbe Formation

The Anisian Kobbe Formation on the southwestern Barents Shelf comprises four coarsening upward clinoform sequences, each separated by three discrete maximum flooding surfaces (Glørstad-Clark et al., 2010; Klausen et al., 2017b). The clinothems contain records of conformably stacked facies associations ranging from organic-rich offshore marine to shallowing upwards deltaic successions. Anisian clinoform surfaces likely developed after repeated gradual progradations of platform deltas punctuating the overall transgressive trend that persisted throughout the Early Triassic in the western Barents Sea (Worsley, 2008; Klausen et al., 2017b). Previous studies have concluded that Anisian sediments in the western and central basin are derived from the southeastern Uralian Provenance, whereas deposits located in areas south of the Loppa High have a prominent Caledonian signature (Mørk, 1999; Bue and Andresen, 2014; Fleming et al., 2016). The seismic attribute map in Fig. 2a shows the geometry of a 1–2 km wide, late Anisian channel located on the Loppa High. The channel is interpreted as a slightly amalgamated distributary channel in a distal position on a mud-rich delta, where the deltatop gradient is low and tidal influence is expected to migrate several kilometers upstream (Klausen et al., 2017b). This is also reflected in palynological signatures from the Nordkapp Basin, where Hochuli and Vigran (2010) found a slightly higher marine influence in the Anisian/Ladinian Kobbe Formation interval compared to the overlying Snadd Formation. Early Triassic climatic records indicate a moderately humid climate (Mangerud and Rømuld, 1991) and both warm temperate and cool temperate characteristics for high latitudes (Ziegler et al., 1994).

2.2. Carnian sedimentation – Snadd Formation

The western Barents Sea region developed from a marine shelf in the Anisian to a paralic platform in the late Carnian (Høy and Lundschien, 2011). Kapp Toscana sediments range from Ladinian to Bajocian/Bathonian in age and are characterized by coarser-grained sediments compared to underlying units (Vigran et al., 2014). The Snadd Formation represents a time-transgressive unit that developed as marginal marine deposits on top of the prograding shelf clinoforms during Ladinian (Riis et al., 2008). Regional sequence stratigraphic development of the Snadd Formation was thoroughly investigated by Klausen et al. (2015) and facies associations ranging from offshore shale through shallow marine to fluvial regimes were described. Most sediment derived from the southeastern Uralian source and was transported into the basin via large-scale (5–20 km wide) channel systems during periods of platform emergence (Glørstad-Clark et al., 2011; Klausen et al., 2014). A variety of fluvial seismic geometries have been documented by Klausen et al. (2014), including point-bar systems in high-sinuosity, meandering channel belts and low-sinuosity, ribbon channel fills, as exemplified in Fig. 2b. It is possible that the northern extension of the Ural orogeny, Novaya Zemlya, became a source area for sedimentation on the Barents Shelf in Middle Triassic (Mørk, 1999). Geometries and spatial distributions of Carnian aged De Geerdalen Formation channel deposits on the Hopen island was studied by Klausen and Mørk (2014) and Lord et al. (2014). These authors documented a combination of massive, highly cross-stratified, laterally accreting sandstone bodies representing fluvial deposits, and heterolithic, stacked channel systems indicative of a tidally influenced paralic depositional environment. Several smaller channel bodies were also recognized and interpreted to represent a distributive part of the delta system.

Seismic offlap break trajectories strongly indicate a general aggrading to slightly prograding depositional style with a gentle platform slope (Høy and Lundschien, 2011; Glørstad-Clark et al., 2010, 2011). Thus, repeated cycles of sea level rise and fall would likely submerge and emerge areas on the Triassic platform over several hundred kilometers inland. Brackish- and fresh water green algae have been documented in the Nordkapp Basin from the Anisian/Ladinian to Late Carnian intervals (Hochuli and Vigran, 2010). The Carnian stage is divided into an early Carnian dry period and a late Carnian humid and warmer period, abruptly separated by the “Carnian pluvial event” (Hochuli and Vigran, 2010; Mueller et al., 2016). Calcite nodules, hematite and goethite has been documented in Carnian palaeosols, which suggests seasonal variations in soil moisture, potentially related to fluctuating groundwater levels (Stensland, 2012; Enga, 2015; Haugen, 2016).

3. Materials and methods

3.1. Dataset

The study is based on core material from the Anisian Kobbe and Carnian Snadd formations in five wells located within different basin configurations in the southwestern Barents Sea (Fig. 1b-c, Table 1). Parameters investigated during sedimentological logging of the core material were lithology, grain sizes, sedimentary structures, unit thicknesses and unit boundaries.

3.2. Sample preparations

Six samples from the Kobbe Formation and 49 samples from the Snadd Formation were collected from facies interpreted as fluvial channels with varying degree of tidal influence. Where possible, samples were collected close to intervals previously sampled for core plug analyses. Thin sections were prepared at the Department of Geosciences (University of Oslo) and all sandstone samples were prepared for powder X-ray diffraction (XRD). Consolidated rock samples were crushed down to smaller particles in a mortar and later milled in a McCrone micronizer for 12 min, using 3 g of sample material liquidized in 9 ml ethanol. The micronized material was left to dry overnight in a cupboard heated to 50 °C. The dried material was carefully loaded in a

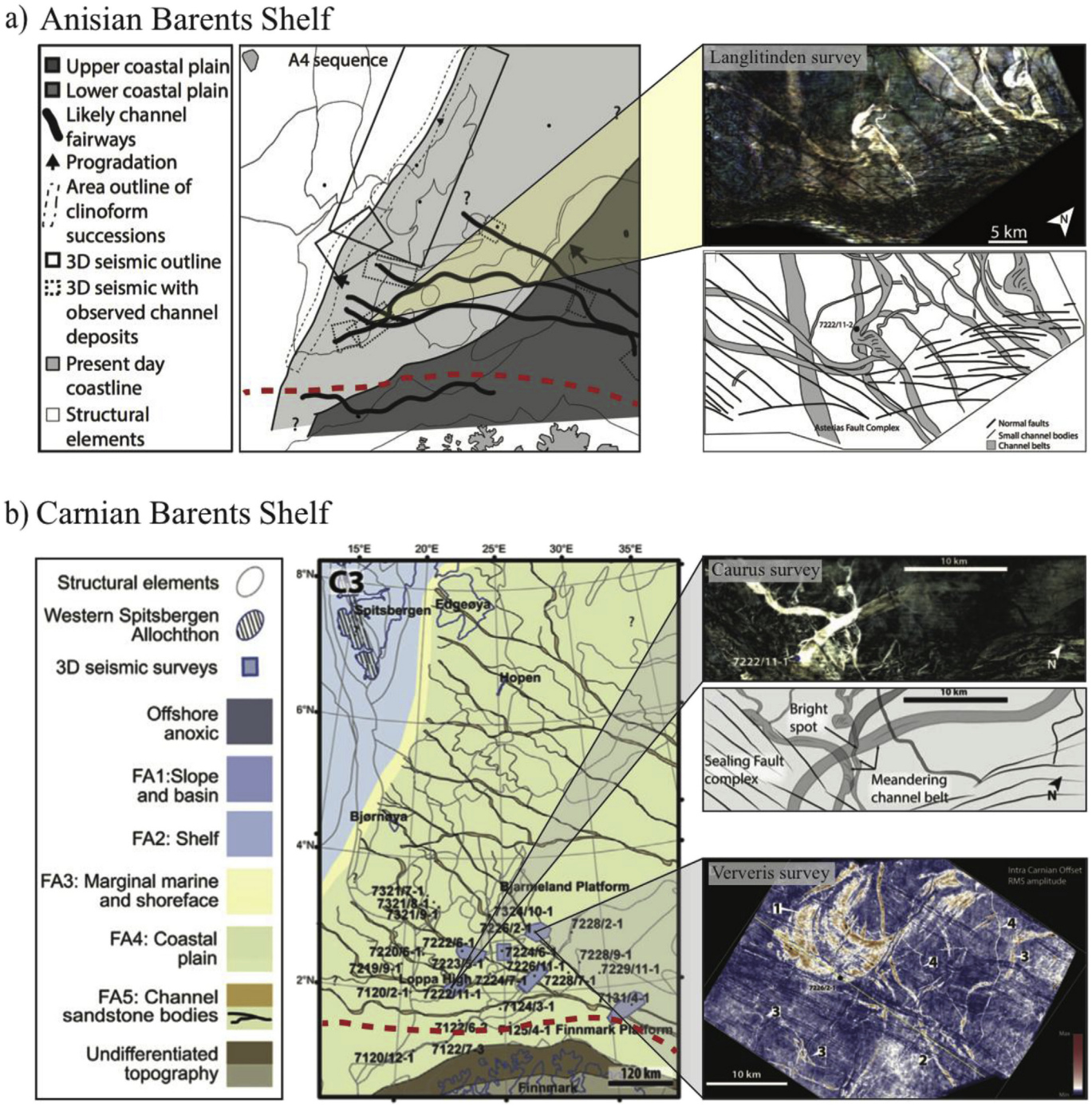

Fig. 2. a) Palaeogeographic reconstruction of the fourth Anisian sequence after Klausen et al. (2017b), seismic attribute map of the Kobbe Formation channel at Loppa High investigated in this study (Langlitinden survey) and associated interpretation after Klausen et al. (2017b). b) Reconstruction of the southwestern Barents Shelf during the third Carnian sequence, after Klausen et al. (2015). RGB-blended spectral-decomposition volume from the Caurus survey (with interpretation) and RMS attribute map from the Ververis survey show various Carnian channel signatures at Loppa High and the Bjarmeland Platform (Klausen et al., 2014, 2015). Red dashed lines indicate the approximate northern distribution limit of the Caledonian sand type, as proposed by Fleming et al. (2016). (For interpretation of the references to color in this figure legend, the reader is referred to the Web version of this article.)

sample holder, ensuring a random orientation of the particles. A D8 Bruker Powder X-ray diffractometer was used to collect data from 2 to 65 °2θ with a step size of 0.01° and a count time of 0.3 s per step. Instrumental parameters for the D8 Bruker device are listed in Table A1 in Appendix. Scanning electron microscopy (SEM) analyses were conducted in the Department of Geosciences at the University of Oslo, on a subset of 11 samples representing channelized deposits from both Kobbe and Snadd formations. A JEOL JSM-6460LV scanning electron microscope equipped with LINK INCA Energy 300 (EDS) and a standard wolfram filament of 15 kV from Oxford Instruments was used during this study.

3.3. Mineral quantification and distribution

Relative quantification of mineral phases from X-ray diffraction data was modelled and analyzed using Rietveld refinement through the software BGMN-Profex (raw data presented in Appendix). Due to complexity in clay mineral structures, quantitative measurements of

Table 1
Core location, depths, age intervals and number of samples collected from the Kobbe and Snadd Formation database presented in this study. Samples from the Snadd Formation account for 90% of the petrographic database.

Well	Location	Core interval [m MD]	Age	Formation	Samples
7228/7-1 A	Nordkapp Basin	2059–2102	Early Carnian	Snadd	18
7321/7-1	Fingerdjupet Sub-basin	2386–2395	Late Carnian/Norian	Snadd	2
7226/2-1	Bjarmeland Platform	1365–1418	Early Carnian	Snadd	18
7222/11-1	Loppa High	778–807	Late Carnian	Snadd	11
7222/11-2	Loppa High	2095–2132	Late Anisian	Kobbe	6

specific clay phase abundances from bulk XRD results have to be treated with care based on these analytical approaches.

Mineralogical and textural characteristics were described through modal analysis on 400 counts per thin section. Compositional variations are illustrated in quartz-feldspar-lithics (QFL) diagrams, where monogranular grains (e.g. quartz, K-feldspars, plagioclases, biotite, muscovite) are distinguished from polygranular grains, termed lithic rock fragments (e.g. microcrystalline chert, igneous/volcanic epiclasts, mica schist and recycled sedimentary rocks). Completely dissolved and recrystallized framework grains, termed pseudomorphous replacements, were treated as part of the rock fragment assembly. Distribution and amount of allogenic matrix, authigenic minerals (e.g. quartz, chlorite, kaolinite, illite and various carbonate minerals) and intergranular porosity were also quantified through modal analysis.

The longest axis of > 100 grains were measured in each sample to produce grain size distribution plots, and the sorting parameter was calculated from the grain size measurements using the standard deviation method after Folk (1980). Grain contacts of > 100 grains were investigated using the visual comparator after Santin et al. (2009) in order to qualitatively evaluate the degree of mechanical compaction in the sandstone samples.

3.4. Characterization of clay mineral morphology and chemistry

Secondary electron (SEI) and back-scattered electron (BEI) analyses were conducted on gold-coated stubs and carbon-coated thin sections using the JEOL JSM-6460LV scanning electron microscope. Elemental mapping analyses were also conducted on carbon-coated thin sections. Elemental distributions of Si, Al, Fe, Na and K were particularly investigated.

3.5. Reservoir quality evaluation

Porosity and permeability values from core plug analyses were obtained from the Diskos National Data Repository by the Norwegian Petroleum Directorate and compared to petrographic observations from modal analyses. Interpretations following comparisons between core plug data and petrographic data must be treated with care, as one is comparing 3D volumes with 2D sections. Helium porosity and horizontal permeability for liquids were used as reservoir quality parameters for the channelized sandstone samples. The cut-off values for reservoir quality evaluation are presented in Table 2.

Table 2
Cut-off values for reservoir quality evaluation used in this study, after Tissot and Welte (1984).

Reservoir quality	Helium porosity [%]	Horizontal liquid permeability [Kl]
Poor	< 10%	< 10 mD
Fair	10%–15%	10–100 mD
Good	15%–20%	100–1000 mD
Very good	> 20%	> 1000 mD

4. Results

Sedimentary and petrographic characteristics of the cored Kobbe and Snadd Formations channels are described separately, followed by a section documenting clay fraction characteristics.

4.1. Anisian Kobbe Formation

4.1.1. Sedimentological characteristics of the cored section

Description: The Anisian core interval from well 7222/11-2 drilled at the Loppa High and shown in Fig. 3, covers a 23-m thick succession of silt and very fine sandstone. The lower 3 m comprises grey shale with thin silt stringers, minor bioturbation and abundant siderite nodules. An 18-m thick unit of very fine to fine sand overlies this unit with an erosive base. Frequently occurring mud clast intervals and cm-scale mud layers are present. Layers of siderite clasts also occur in this unit, notably at the base and in the upper part. The sandstone fines upwards to silt and the unit is overlain by an interval consisting of laminated clay deposits.

Interpretation: The fine-grained deposits in the lower part of the cored succession represent deposition of hypopycnal sediments. Lack of sedimentary structures and bioturbation indicate restricted current conditions and marine influence. The presence of siderite concretions found within the shale are indicative of fresh-to brackish water conditions (Woodland and Stenstrom, 1979) and suggest proximity to a fluvial outlet facilitating supply of Fe^{2+}. An interfluvial bay environment is interpreted for this part of the succession. The frequency of mud clast layers might reflect channel instability. The uppermost heterolithic and plane-parallel laminated shale is interpreted as representing tidal flat and floodplain facies deposited in a delta top environment.

4.1.2. Petrographic character of the Anisian channel

Samples recovered from the Anisian channel show an abundance of quartz and plagioclase, comprising 65–85% of the bulk volume (Fig. 3). Microcline is observed in small amounts (averaging at 1.5%). The most common clay minerals are chlorite and muscovite/illite, and the concentrations of kaolinite range from 0 to 11% of the bulk sample. The total clay mineral content of the bulk sand appears to increase in sandstone intervals containing large mud flakes. Where present, siderite and calcite account for < 1.5% of the bulk. No traces of igneous minerals (e.g. pyroxene, amphibole, epidote, fluorapatite) were encountered in these samples.

The channelized Anisian sandstone is classified as litharenithic (Fig. 4a). The framework is primarily composed of moderately well sorted fine to very fine sand grains and with the majority of grain contacts being long (Fig. 4b). The litharenithic composition indicates that the high plagioclase concentrations registered from the bulk XRD analysis must be contained within the lithic rock fragment assembly. Recycled sedimentary rock fragments, detrital mica and igneous epiclasts are the major components of the rock fragment assembly.

The intergranular volume (IGV) of samples collected from the Anisian channel is presented graphically in Fig. 4c. IGV values range from 18% to 33% (averages at 28%) and allogenic matrix accounts for 40–65% of the IGV. Pore-filling and pore-lining chlorite cement make up 3–13% of the IGV, whereas registered concentrations of kaolinite

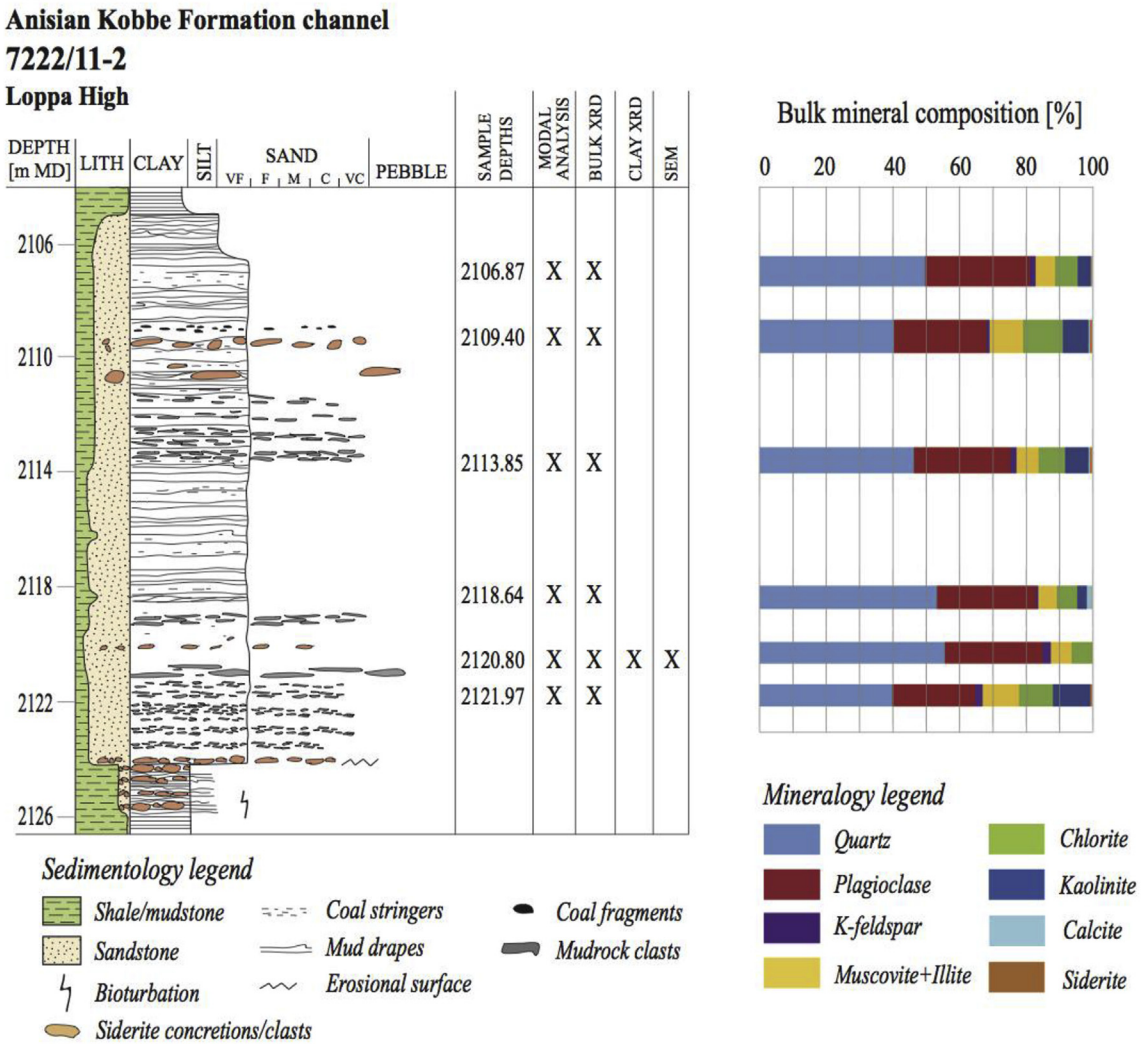

Fig. 3. Left) Logged section and sample locations collected from the Anisian Langlitinden (7222/11–2) core drilled on the Loppa High. Heterolithic lithology, mud drapes and frequent mud clast intervals indicate strong tidal influence and channel instability. Right) Bulk mineralogy from X-ray diffraction data shows a dominance of quartz and plagioclase feldspars, chloritic and kaolin clay minerals and limited distribution of carbonate minerals.

and authigenic quartz cement ranges from 0.75 to 5.5% and 1–2.5%, respectively. The primary porosity obtained from modal analysis ranges between 0 and 3%.

Core plug data from the Anisian channel show that horizontal porosities plot above the cut-off value of 10% for fair reservoir quality (Fig. 4d). However, with horizontal permeability values lower than 10 mD, the channelized Anisian sandstone is characterized as a poor-quality reservoir (Tissot and Welte, 1984). When comparing core plug data with corresponding petrographic results, the sample containing the lowest matrix concentration (2121.97 m MD) displays the highest permeability value of the samples investigated. Although this sample contains the lowest concentration of cements, the low IGV places the core plug sample close to the cut-off boundary for fair porosity. High cement and matrix concentrations result in extremely poor permeability and fair porosity values (2118.85 m MD). Helium porosities approaching 20% are found in samples with less than 10% cement (2120.80 m MD). Matrix content of 15% in this sample limits the permeability below the cut-off value for fair reservoir quality.

The petrographic thin section in Fig. 4e shows the abundance of monocrystalline quartz grains (Qz) mud rock fragments (MRF), partly dissolved framework grains that have transformed into mixtures of illitic and chloritic clay minerals (chl/ill) and allogenic matrix (Mtx). Lithic rock fragments (LRF) and pore-filling chlorite cement (Chl) are also observed. The blue-colored epoxy indicates the porosity in the 2D section. The most common grain contact is long and the grains are sub-angular to sub-rounded.

4.2. Carnian Snadd Formation

4.2.1. Sedimentological characteristics of Carnian cored sections

Description: Heterolithic shale units at the bottom of the cored Carnian sections depicted in Fig. 5 are often associated with < 2 m thick, fine-grained sand packages with large, sub-angular mud and quartz clasts. Homogeneous, fine-grained and crossbedded sandstone overlies the small channel packages and comprise the dominant part of the cored section (22–50 m vertical thickness). Calcite-cemented intervals are frequently observed within the homogeneous section and overprint sedimentary structures. The boundaries between calcite-cemented and non-cemented lithologies are sharp and do not coincide with sedimentary boundaries. The upper boundary of the thick sandstone section was only cored in well 7228/7-1 A from the Nordkapp Basin, where the channelized deposit measure 37 m in vertical thickness (Fig. 5b). This sandstone package is conformably overlain by a 20-cm thin, mottled shale unit.

Interpretation: The lowermost heterolithic shale units are interpreted as floodplain deposits that were cut by distributary channels, equivalent

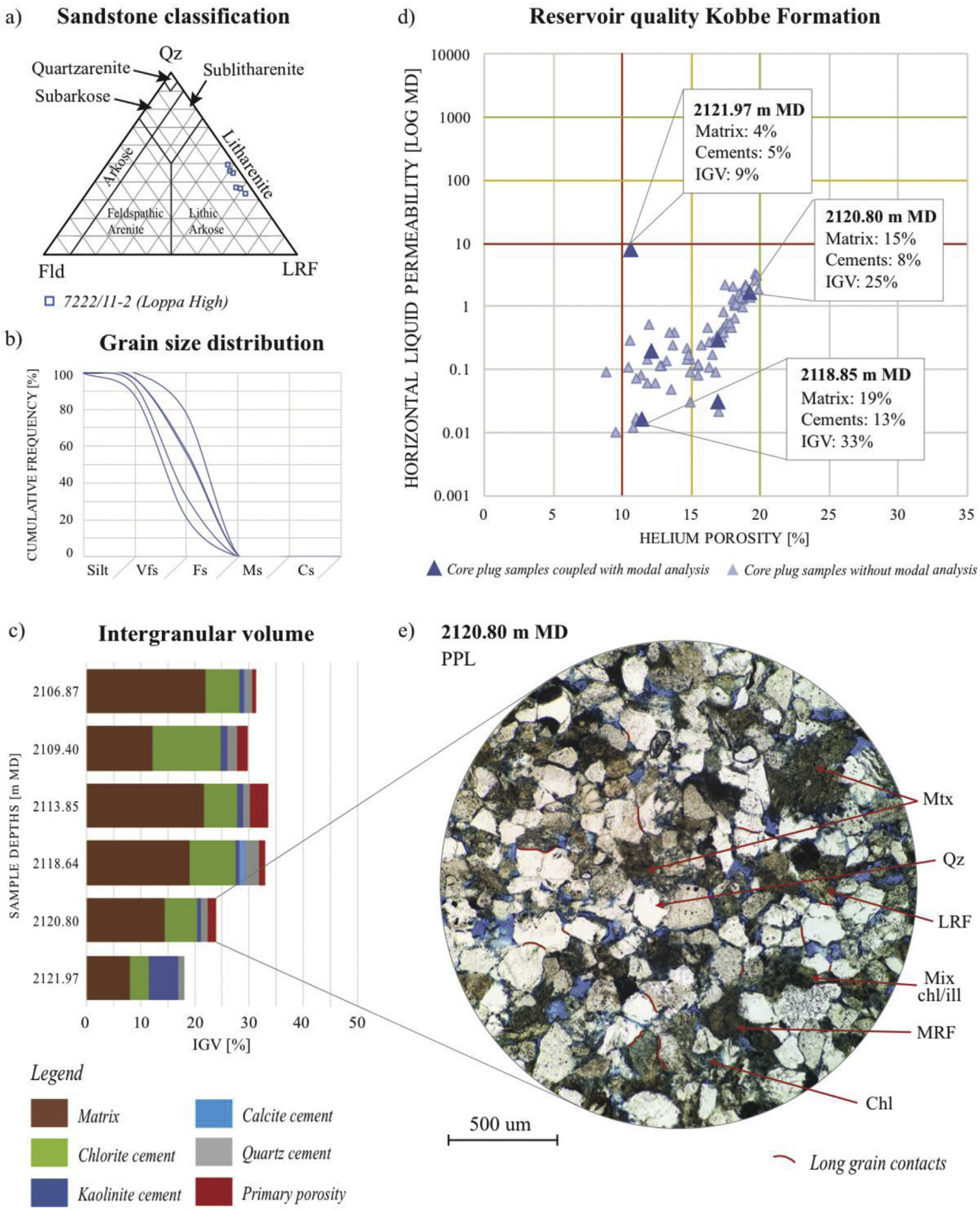

Fig. 4. Petrographic characteristics of samples collected from the Anisian Kobbe Formation channel at the Loppa High. a) The QFL diagram shows that all sandstone samples classify as litharenites. b) Grain size distribution plot of very fine to fine sandstone from the Kobbe Formation channel. The shape of the curve indicates moderate to well sorting. c) Detrital matrix fills about 70% of the intergranular volumes (IGV) registered in the Kobbe Formation channel. d) Horizontal liquid permeability versus Helium porosity from core plug data. Reservoir quality is defined based on cut-off values: poor (red), good (yellow) and very good (green). Most samples show good porosity values, but due to poor permeability the Kobbe Formation classify as a poor-quality reservoir. e) Petrographic thin section image from a sample located at 2120.80 m MD, with blue epoxy impregnation. Long grain contacts are indicated in red lines. PPL = Plane polarized light, Mtx = Matrix, Qz = Quartz, LRF = Lithic rock fragments, Chl = chlorite, ill = illite, MRF = mud rock fragment. (For interpretation of the references to color in this figure legend, the reader is referred to the Web version of this article.)

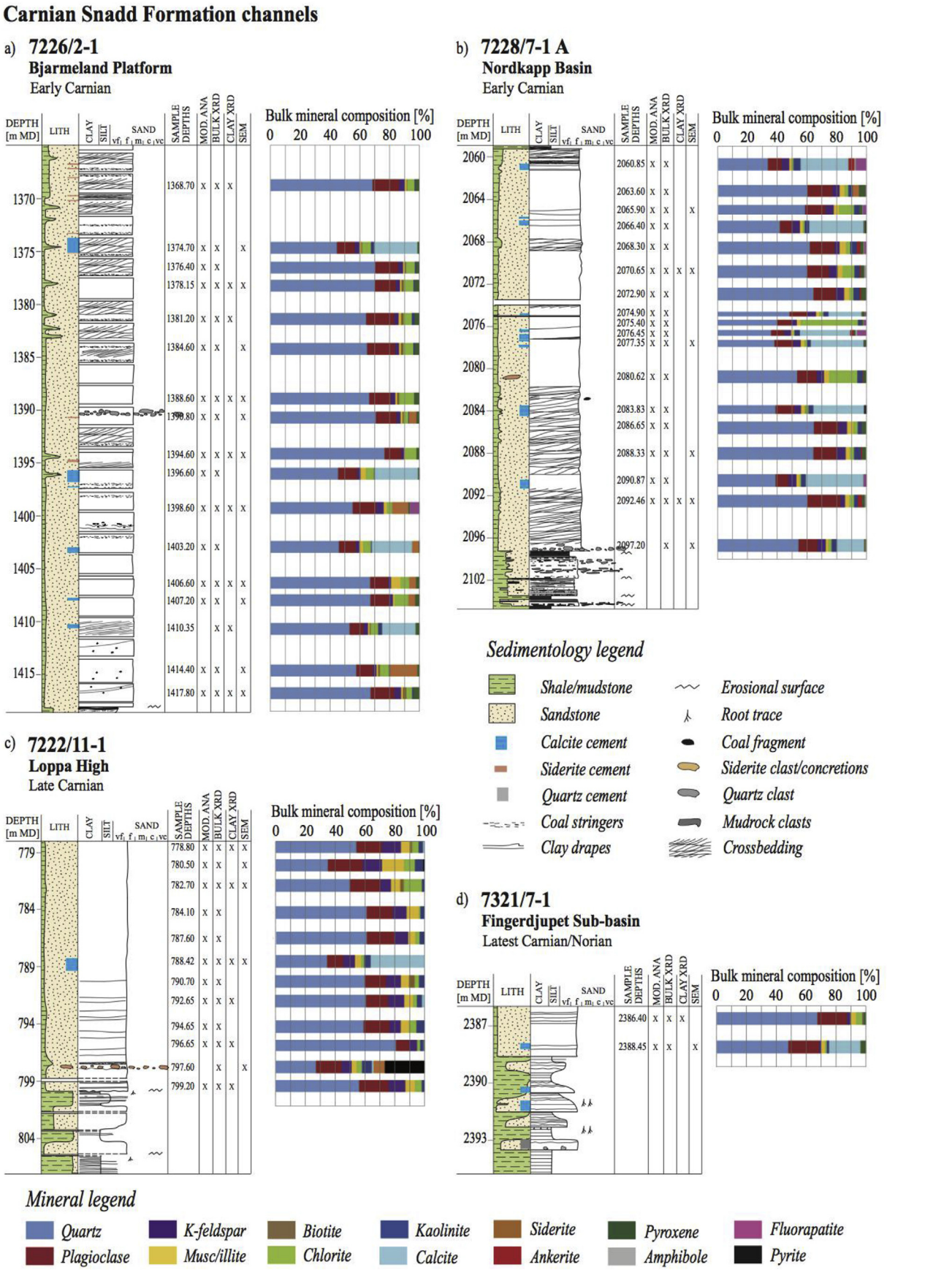

(caption on next page)

Fig. 5. Sedimentary features, sample overview and bulk XRD mineral assemblies from the Carnian channels cored in the a) Bjarmeland Platform (Early Carnian), b) Nordkapp Basin (Early Carnian), c) Loppa High (Late Carnian) and d) Fingerdjupet Sub-basin (Latest Carnian/Norian). The core signature is dominated by fine to medium-grained cross-beds alternating with massive sandstone lacking any primary sedimentary structures. Coal fragments and clay stringers occur frequently. Coarse conglomerates with mudrock clasts and/or quartz pebbles usually occur at the base of the channelized sections. The dominating minerals are quartz and plagioclase, and chlorite is the dominating clay mineral. Calcite-cementation occur at irregular intervals.

to the smaller channel bodies documented at the Hopen island by Klausen and Mørk (2014) and Lord et al. (2014). The crossbedded and homogeneous sections are interpreted as channel fills and fluvial dune deposits in deep, stable channels that developed on the delta top during the Middle – Late Triassic. We interpret the smaller distributary channel units to represent the first sequence of channel erosion on the delta plain, deposited prior to the establishment of the deep and stable channel belts. Channel belt systems have been detected on seismic data across large distances on the southwestern Barents Shelf (Klausen et al., 2014, 2015) and in outcrops analogues on the Svalbard archipelagos (Klausen and Mørk, 2014; Lord et al., 2014). Clastic sediments deposited in these channel systems likely constitute a combination of suspended load and bedload from the provenance, mixed with erosional products from the floodplain upstream. Homogeneous and fine-grained particles might testify to long transport distances. The mottled shale unit overlying the deep channel in the Nordkapp Basin is interpreted as a palaeosol section.

4.2.2. Petrographic character of Carnian channels

Quartz and feldspars make up > 80% of the average mineral assembly in the Snadd Formation channels in this study. Plagioclase is the most common feldspar and accounts for 10–20% of the bulk in all channels. The concentration range of K-feldspar varies with location; 5–13% at the Loppa High (Fig. 5c), 3–6% in the Nordkapp Basin (Fig. 5b) and 1–4% in the northernmost wells (Fig. 5a and d). The dominating clay mineral is chlorite, mostly ranging in concentration from 5 to 10% of the bulk sample. Muscovite accounts for 2–3%, although slightly higher concentrations (5–8%) were encountered in the channel on the Loppa High. Less than 2% biotite was observed in samples from the Bjarmeland Platform and in a few samples from the Loppa High. Kaolinite concentrations range from 2 to 5% in the Nordkapp Basin and Loppa High channels, but only trace amounts of kaolinite were observed in channels from the Fingerdjupet Sub-basin and the Bjarmeland Platform. Carbonate minerals such as calcite, siderite and ankerite occur sporadically throughout the Carnian channels. Whenever present, calcite comprises 25–35% of the bulk mineralogy in a sample. Most siderite is observed in the lower part of the channel from the Bjarmeland Platform, where it accounts for 5–15% of the bulk. Ankerite was detected in minor amounts (< 2%) in the Nordkapp Basin channel. Samples from the Carnian channels in the Nordkapp Basin, Fingerdjupet Sub-basin and Bjarmeland Platform contain 0.5–4% pyroxene. Amphibole and fluorapatite were only observed in the Nordkapp Basin channel and usually account for < 1% of the bulk mineralogy.

The Carnian channels are classified as litharenites, but samples from the Bjarmeland Platform and Loppa High display slightly more mature compositions compared to channels in the Nordkapp Basin and Fingerdjupet Sub-basin (Fig. 6a). A few samples from the Bjarmeland Platform classify as sub-litharenites. Slightly higher feldspar content is noted for the channel on the Loppa High. Lithic rock fragments are usually detrital chert grains, recycled sedimentary fragments, mica grains and metamorphic/igneous epiclasts. These grains generally show poor preservation (secondary pores and rough surfaces). Medium to fine-grained sand is registered within the channels from the Fingerdjupet Sub-basin and Nordkapp Basin, fine-grained sandstone beds dominate the Bjarmeland Platform channel and very fine to fine-grained sandstone beds dominate the Loppa High channel of the Snadd Formation (Fig. 6b). The most common grain contact in the channels from the Nordkapp Basin and Fingerdjupet Sub-basin is long, whereas tangential grain contacts dominate in the Loppa High and Bjarmeland Platform channels.

The helium porosity versus permeability plot in Fig. 6c shows that most samples from the Carnian channels in this study contain porosity values defined as very good (> 20%). Liquid permeability values plot above good quality (> 100 mD). Samples that plot within the poor reservoir quality area, showing both low porosity and permeability, are carbonate-cemented. Samples from the Carnian channel at Loppa High display the best reservoir quality, with measured porosities above 30%. The Nordkapp Basin channel data show slightly more varied reservoir quality, but a clear trend between porosity and permeability is observed. The channel on the Bjarmeland Platform shows consistently good reservoir quality. Inset boxes in Fig. 6c show matrix content, cement concentration and IGV for a few sandstone samples in the dataset. There appears to be a relationship between matrix content and reservoir quality, where samples with the best reservoir quality contain limited amounts of detrital matrix. However, matrix concentrations up to 16% (as seen in the sample at 1406.60 m MD from the Bjarmeland Platform) appear to be acceptable for good quality reservoirs. Siderite cement up to 10% appears to have limited effect on the reservoir quality. Pore-filling chlorite cement and detrital matrix reduces both helium porosity and liquid permeability values in the Nordkapp Basin sample.

Non-cemented samples from the Carnian channels show an average IGV of 29% (Fig. 7). The average amount of matrix material varies between the channels; < 3% on the Loppa High (Fig. 7c), 5% in the Nordkapp Basin (Fig. 7b), 9% on the Bjarmeland Platform (Fig. 7a) and 12% in the Fingerdjupet Sub-basin (Fig. 7d). Chlorite and kaolinite make up an average of 12% in the Carnian channel on the Loppa High, 8% in the Nordkapp Basin and Fingerdjupet Sub-basin channels and 4% in the Bjarmeland Platform channel. Quartz cement comprises < 3% in all samples. The average primary porosities obtained from modal analysis range from 10 to 13%. The average IGV of the carbonate-cemented samples is 40% in the Nordkapp Basin channel, 31% in the Fingerdjupet Sub-basin, 38% on Loppa High and 34% in the channel at the Bjarmeland Platform. Pore-filling cements are mostly calcite, but these samples also contain minor amounts of siderite, chlorite, illite and kaolin cements. The average porosity in the cemented samples is < 3%.

The petrographic thin section from the Carnian channel on the Bjarmeland Platform shows slightly higher compositional maturity compared to the other Carnian channels, and both tangential grain contacts (Fig. 7e) and long grain contacts are observed in these sandstones. Samples from the lower half of this channel are characterized by clusters of Fe-rich, zoned sphaerosiderites (Sphr.siderite) and smaller spheroidal siderites. Both siderite types are attached to chlorite-coated, detrital quartz grains. These cements are included as part of the intergranular volume and are also observed in samples from the Nordkapp Basin.

Fig. 7f shows the typical immature composition of a sample from the Nordkapp Basin as seen in crossed polarized light (XPL). The grains are sub-angular and the most common grain contact is long. Pseudomorphous replacements (PsMR) are grains where fine-grained chlorite has replaced precursor minerals of detrital framework grains, while preserving the shape of the original grain (Fig. 9a-b). Other dissolved rock fragments are replaced by pore-filling chlorite and kaolinite cements.

The sample from the channel studied at the Loppa High shows immature sandstone composition with sub-angular grains and tangential grain contacts (Fig. 7g). Dissolution of framework grains is common and higher bulk kaolinite content is registered in this channel compared

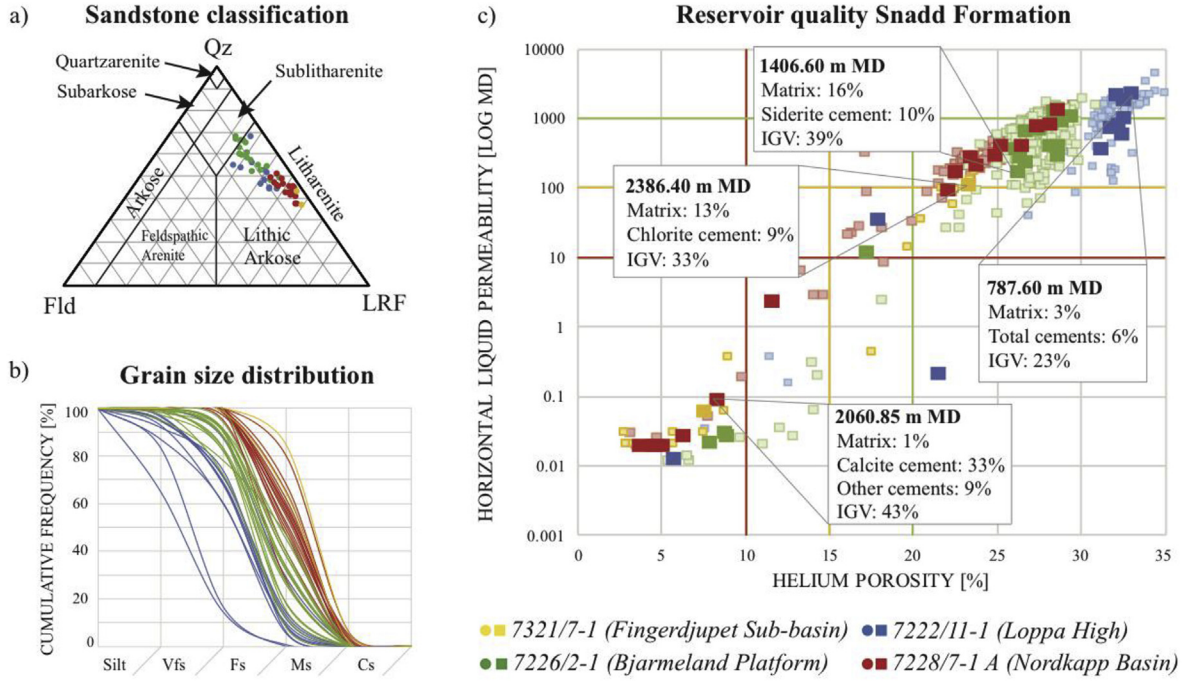

Fig. 6. Petrographic characteristics of samples from the Carnian channels. a) The QFL-diagram after Folk (1980) classifies most samples as lithic arenites, but the samples from the Bjarmeland Platform show a more mature composition. b) The grain size distribution graph shows variety from very fine to medium-grained sand. There appears to be a correlation between grain size and location, where the grain size is coarser in the Fingerdjupet Sub-basin and finer on the Loppa High. c) Horizontal liquid permeability versus Helium porosity from core plug data. Cut-off values are the same as in Fig. 4 and most Snadd Formation samples plot within the good reservoir quality field. Highlighted colors represent point-counted samples. Poor-quality samples are associated with calcite cementation. Matrix values up to 16% are acceptable for good-quality reservoirs with high IGV.

to the other Carnian channels (Fig. 7c). Rock fragments are composed of mineral aggregates of K-feldspar, quartz and chlorite (Figs. 8, 9g-h). Albite is often the remaining material outlining the original shape of the detrital framework grain (Figs. 9c-d, 9g-h).

4.3. Clay fraction characteristics in Anisian and Carnian channels

The clay fraction in the Carnian and Anisian channels is dominated by chloritic clay minerals, but kaolin was also identified from XRD, SEM and modal analyses. Most clay material is distributed as pore-filling crystals, often within proximity to partially dissolved rock fragments. Pore-filling chlorite crystals often display pipe cleaner morphologies or bridges between detrital grains (Fig. 10a), whereas kaolin minerals (kaolinite and dickite) are characteristic by their stacked booklet morphology.

Well-developed chlorite coatings were observed in SEM and are characterized by two coating generations (Fig. 10b): The first-generation coating (Chlorite 1) consists of a chloritic material with small, anhedral crystals that fill in indentations of grain surfaces. Large thickness variations are observed for the first-generation coating and a sub-parallel orientation to the grain surface is registered. The second-generation chlorite (Chlorite 2) displays larger, euhedral crystals and show a growth orientation perpendicular to the grain surface. Carnian channel sandstones from the Fingerdjupet Sub-basin contain euhedral crystals with thickness up to 12 µm, whereas euhedral coating thicknesses between 2 and 6 µm are registered in the other channels of this study.

The grain coating coverage appears to be complete on most grain surfaces in the Snadd Formation (Fig. 10c), whereas chlorite coatings are less developed in the Kobbe Formation. Large chlorite crystals are absent at grain-to-grain contacts, but smaller crystals have been observed in these areas through SEM (inlet micrograph in Fig. 10c). Chlorite coatings are also observed in calcite-cemented samples (Fig. 10d) and around secondary pore space, outlining the shapes of completely dissolved grains (Figs. 9a-b, 9g-h).

5. Discussion

The discussion based on this study will focus on; 1) the relationship between provenance, initial sandstone composition and distribution of precursor clay coatings, 2) the relative impact of early diagenesis and mechanical compaction on reservoir quality, and 3) palaeo-temperatures indicated from clay mineralogy.

5.1. Sandstone provenance and composition

Previous studies describe Middle – Late Triassic sandstones north of the Hammerfest Basin as immature and compositionally varied, with abundant concentrations of polygranular rock fragments. Reported rock fragment assemblies throughout the basin include polycrystalline metamorphic fragments, metasediments (e.g. schists), micas, chert and granitic grains (Bergan and Knarud, 1993; Mørk, 1999; Fleming et al., 2016). The abundant minerals in the Snadd and Kobbe formations are quartz and albite, whereas the distribution of K-feldspar is limited. Observed accessory minerals are pyroxene, epidote and black ore minerals, but these are mostly restricted to the Carnian Snadd Formation sandstones located in the eastern areas of the Barents Shelf. Kaolinite, chlorite and mica/illite dominate the clay fraction throughout the basin, but smectitic clays have been observed in Carnian deposits in the northern and eastern regions of the Barents Shelf (Bergan and Knarud, 1993; Mørk, 1999). Mineralogical results from previous investigations comply well with the results from the present study, indicating a common provenance. Detrital zircon age signatures from the Late Triassic De Geerdalen Formation on the Svalbard archipelagos contain populations of Carboniferous and Permo-Triassic age signatures that have been linked to the Uralides and Taimyr source areas (Bue and Andresen, 2014). As sandy equivalents of the Anisian Kobbe Formation never reached the northern position of the present-day Svalbard

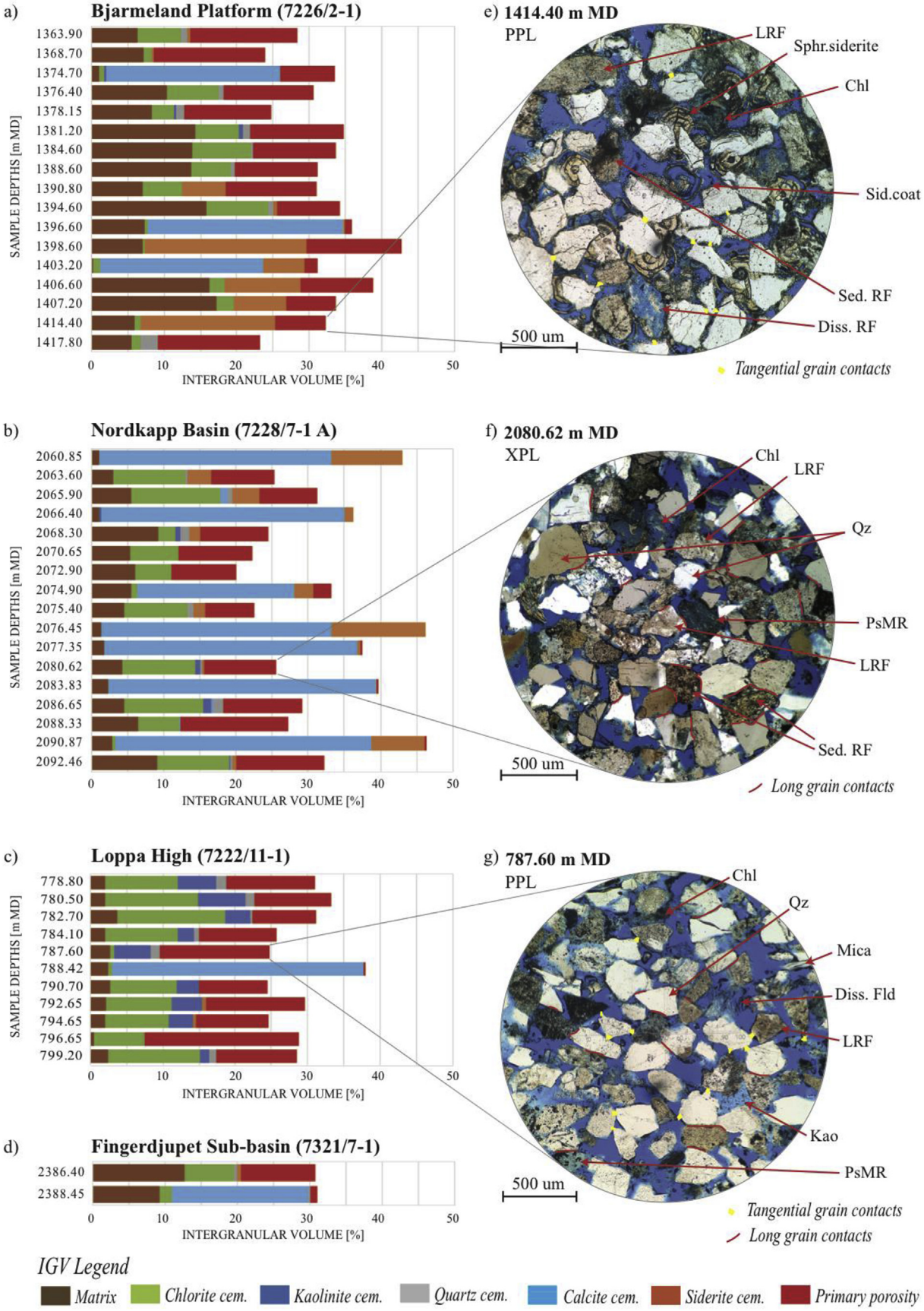

(caption on next page)

Fig. 7. Intergranular volumes for Carnian channel samples (presented in m MD) located in the a) Bjarmeland Platform, b) Nordkapp Basin, c) Loppa High and d) Fingerdjupet Sub-basin. Figures e) – g) show petrographic thin sections from three samples. Examples of tangential grain contacts are indicated in yellow dots and long grain contacts are indicated in red lines. Abbreviations: PPL = plane-polarized light, XPL = cross-polarized light, LRF = lithic rock fragments, Qz = quartz, Sphr.side = sphaerosiderites, Chl = chlorite, Sid.coat = siderite coating, Diss.Fld = dissolved feldspar, Kao = kaolinite cement, PsMR = pseudomorphous replacement, Sed. RF = sedimentary rock fragment. (For interpretation of the references to color in this figure legend, the reader is referred to the Web version of this article.)

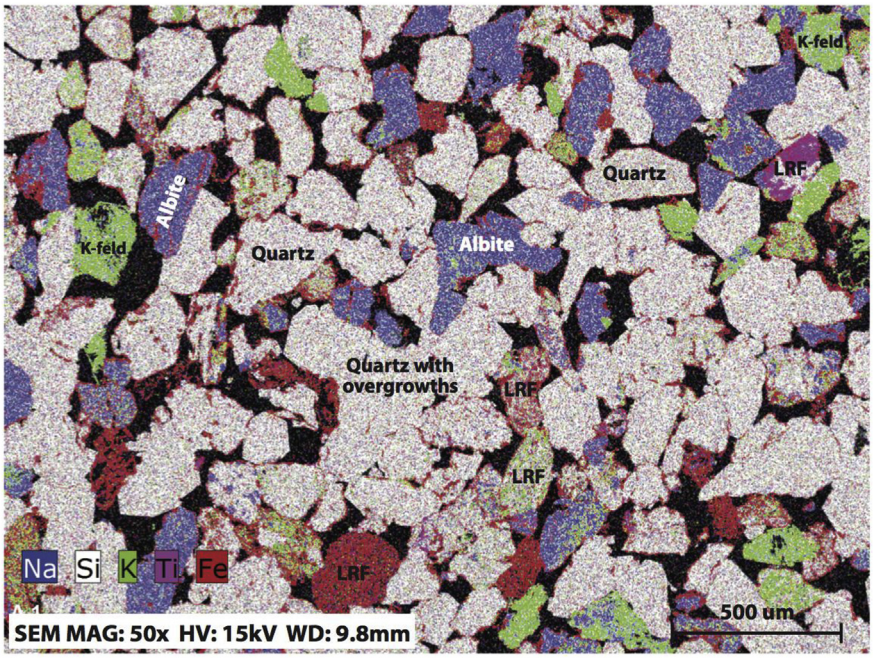

Fig. 8. Elemental distribution map of Na, Si, K, Ti and Fe in a sample from the Bjarmeland Platform (sample depth = 1417.80 m MD) shows the relative abundance of albite grains (blue), chorite coatings and iron-rich clasts (red), quartz grains (white) and K-feldspar grains (green). Lithic rock fragments (LRF) are mineral aggregates of iron-rich minerals, albite, rutile (pink), K-feldspars and quartz, and often display long grain contacts. (For interpretation of the references to color in this figure legend, the reader is referred to the Web version of this article.)

archipelago, we assume a common provenance for both Snadd and Kobbe formations in the southwestern Barents Sea based on the mineralogical similarities documented in this study. Combined with seismic evidence of northwestward prograding clinoforms in the southwestern Barents Sea during the Triassic (Glørstad-Clark et al., 2010, 2011), most data point towards a southeastern Uralide provenance for the Middle – Late Triassic sandstones in this study.

The hardness of albite and microcline (6.0–6.5) would suggest that the physical endurance of feldspars is comparable to that of quartz (hardness 7.0). This implies that, in terms of physical transport, fine-grained sandstones comprised of 70–80% quartz and plagioclase, as documented in the present study, could be considered as a physically mature sediment. The general consensus state that reservoir quality in Uralian-sourced sandstones in the Barents Sea is challenging to predict due to compositional variability (Fleming et al., 2016). In published literature, sandstones north of the Hammerfest Basin vary from feldsarenites and lithic arkoses to feldspathic arenites and litharenites, representing the whole range of sandstone classes with less than 80% quartz (Fig. 11). Plagioclase dominates over K-feldspar in sandstones investigated by Bergan and Knarud (1993), Haile et al. (2017) and in the present study, whereas Mørk (1999) registered K-feldspar as the dominant feldspar. Clearly, sandstone classification from modal analysis is prone to inconsistent registration due to poor preservation of twins in feldspar grains, making feldspar separation difficult in microscope. Untwinned feldspars may thus represent a characteristic feature of the Uralian provenance. Mapping of aggregate grains in this study revealed a significant amount of feldspathic minerals as dominant constituents of the rock fragment assembly (Figs. 8 and 9). Sandstone classification diagrams, e.g. Folk (1954) and Dott (1964), would be affected by inconsistent separation between feldspar-rich lithic rock fragments (e.g. polycrystalline granitic grains) and detrital, monocrystalline feldspar grains, as exemplified by litharenithic samples from the present study (colored circled in Fig. 11). In the present study, it appears as the bulk XRD results are better aligned with elemental distribution maps obtained from SEM, compared to results from modal analysis. As modal analysis is considered semi-quantitative and prone to subjective interpretation, such analyses should be coupled with SEM and XRD analyses, and detailed facies descriptions. Most publications do not make a clear facies distinction when describing Triassic sandstones from the southwestern Barents Sea petrographically, which could also account for the observed compositional variability depicted in published literature (Fig. 11).

5.2. Emplacement of precursor clay coatings in fluvial sandstones

While pore-filling chloritic clays generally have a negative impact on the reservoir quality, the presence of grain coating chlorite is considered a necessity for preserving porosity in sandstones exposed to temperatures exceeding 70 °C (Ehrenberg, 1993; Walderhaug, 1996; Bloch et al., 2002). In the following section we discuss the physical emplacement process of the precursor clay material on detrital grain surfaces. The precursor material is not to be confused with the crystalline chlorite coatings documented in this study (Fig. 10), which represent the diagenetic overprint of the detrital coating precursor.

As grain-coatings were observed in completely calcite-cemented samples with IGV values in the range of 33–40% (Fig. 10d), petrographic relations suggest that the emplacement of the precursor coating pre-dates the formation of early carbonate cementation. The first-generation coating is thicker in grain surface indentations and the precursor clay was likely emplaced on the grain surfaces prior to significant sediment packing. Small chloritic crystals observed at grain-to-grain contacts indicate movement of the grain framework simultaneously with the onset of the coating emplacement process. Few empirical studies exist on the physical mechanisms for emplacing clay coatings on detrital sand grains, but Matlack et al. (1989) found that four criteria facilitated such a process: 1) coarse sediment, 2) high

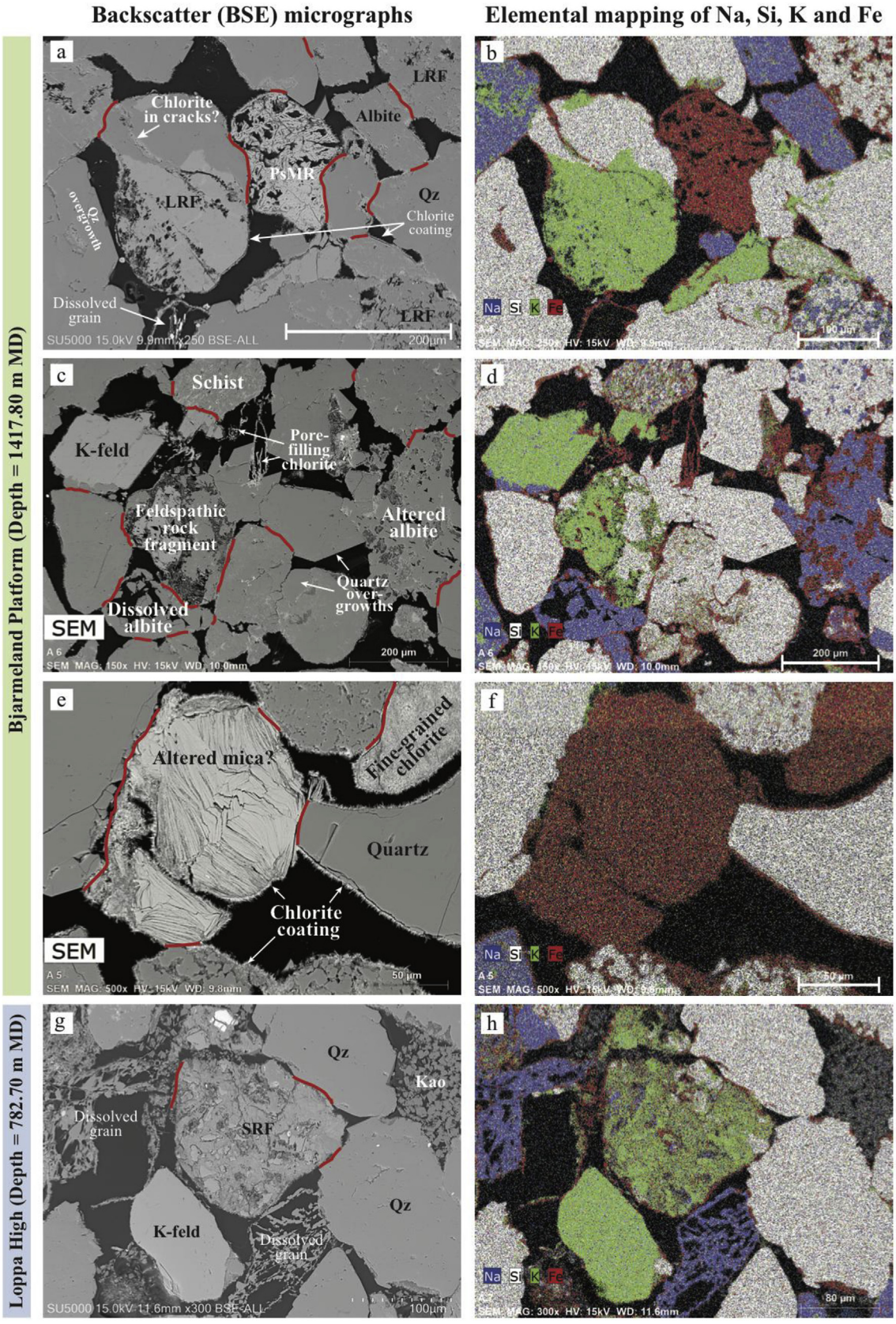

(caption on next page)

concentrations of clay in suspension, 3) fluctuating water levels and 4) little sediment reworking. These criteria raise several implications for the Triassic channels in this study:

1) The first criteria would suggest that the Uralian-sourced Anisian and Carnian channels display grain sizes too small for grain coating emplacement to be efficient. The presence of well-developed grain

Fig. 9. Backscatter (BSE) micrographs and elemental mapping of Na, Si, K and Fe from two Snadd Formation channels located at the Bjarmeland platform (a–f) and Loppa High (g–h). a) – b) Lithic and sedimentary rock fragments consist of mineral aggregates of quartz, K-feldspar and iron-bearing minerals that produce long grain contacts (indicated with red lines). Chlorite coating is almost completely distributed around framework grains. Pseudomorphous replacements (PsMR) solely consist of iron-rich, authigenic chloritic cements with ductile deformation response to mechanical stress. c) – d) Quartz overgrowths grow into the intergranular pore space. Rock fragments containing K-feldspar (green) and albite (blue) are significantly altered. Albite is also found as overgrowth on detrital K-feldspar grain (seen on the left). e) – f) Altered mica clast replaced by iron-rich authigenic cement (chlorite?). Chlorite coating crystals are well-defined and distributed around detrital framework grains. g) – h) Albite is often the remnant material that outlines the shape of dissolved framework grains. Abbreviations: LRF = lithic rock fragment, PMR = pseudomorphous replacement, SRF = sedimentary rock fragment, Qz = Quartz, K-feld = K-feldpar (microcline), Kao = Kaolinite. (For interpretation of the references to color in this figure legend, the reader is referred to the Web version of this article.)

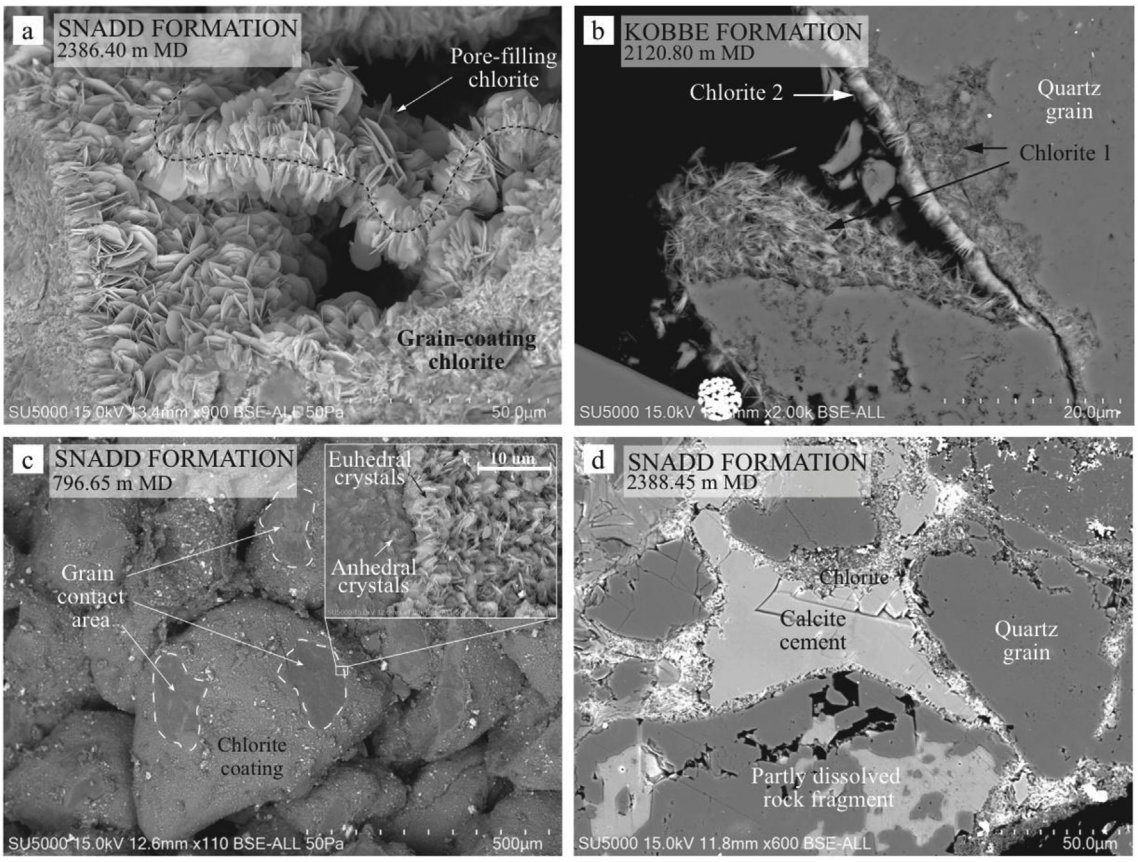

Fig. 10. Backscatter (BSE) micrographs showing chlorite coating characteristics in Anisian and Carnian channels. a) Pore-filling chlorite often display "pipe cleaner" morphology or bridges between detrital grains (indicated by black dashed line). b) Two generations of chlorite coatings are observed on a detrital quartz grain in the Kobbe Formation channel at Loppa High: small, anhedral first-generation coatings (Chlorite 1) and larger, euhedral second-generation coatings (Chlorite 2). c) High grain-coating coverage of framework grains was registered in the Snadd Formation channel at the Loppa High. Grain-to-grain contact areas (highlighted by dashed white lines) are coated with small, anhedral chlorite crystals (inlet micrograph). d) Chlorite coating was observed rimming detrital framework grains in a calcite-cemented sample (IGV = 34%) from the Carnian Fingerdjupet Sub-basin channel.

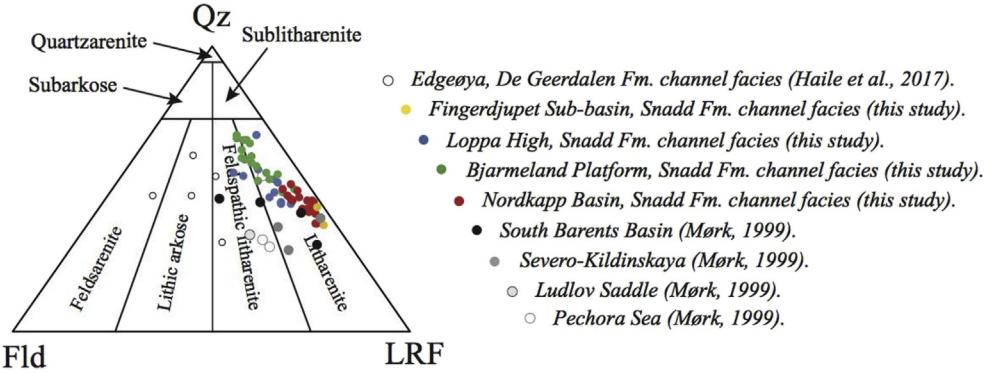

Fig. 11. Sandstone classification diagram (Folk, 1954) showing Snadd Formation samples in this study (colored circles) compared to published results from modal analyses of Middle – Late Triassic samples in various basin locations after Mørk (1999) and Haile et al. (2017). By registering feldspar-rich granitic grains as lithic rock fragments, samples from the present study are placed in the litharenithic class. Mørk (1999) included polygranular quartz grains in the lithic rock fragment assembly, and thereby placing the samples closer to the lithic rock fragments (LRF) axis compared to studies without the mono-polycrystalline distinction. Sedimentary facies were not distinguished. Samples from Haile et al. (2017) appear significantly more feldspar-rich, which could be an effect of the distal position of Edgeøya relative to the Uralide provenance.

coating chlorite in fine-grained Kobbe and Snadd formation sandstone beds contradicts the statement. In a recent study of grain coatings in the Ravenglass Estuary, NW England, Wooldridge et al. (2017) found that fine-grained sediment together with > 5% matrix content facilitated development of uniform, well-developed clay coats on detrital grains. As the coating in the Kobbe Formation channel is thinner relative to the coatings in the coarse-grained Carnian channels, sediment grain size might still impact the coating thickness. Thin grain coatings would be preferable in regards to reservoir quality, as they have reduced effect on the pore neck diameters, which influence the sandstone permeability. This effect is not observed in the data presented in this study, as the permeability values registered in the Kobbe Formation channel is significantly lower compared to the Snadd Formation channels. The coating thickness effect on permeability in the studied samples is believed to be camouflaged by high concentrations of pore-filling matrix that have a significantly higher impact on reservoir permeability.

2) With the Triassic Barents Shelf being characterized as a clay-rich and low-gradient deltaic system (Klausen et al., 2017b), high suspended clay concentrations in the Anisian channels would be expected. Both the Carnian and the Anisian delta systems were likely very sensitive to sea level variations, and tidal influence is believed to migrate several kilometers upstream during sea level highstand. In this scenario, tidal currents could facilitate deposition of suspended clay particles into the channelized sand by counteracting and stagnating the fluvial current, making settling of the suspended clay material possible. Physical disaggregation of lithic aggregate grains and mud rock fragments eroded from the floodplain is also believed to contribute to high suspended clay concentrations in the channels.
3) Sedimentary structures observed in the Anisian channel at Loppa High would suggest a strong tidal component in this channel and thereby attest to fluctuating conditions. Strong tidal influence could also explain the high matrix concentrations documented in this channel. The Carnian Snadd Formation channels show very few sedimentary structures that would attest to a strong tidal influence, but sporadic occurrence of calcite cement would suggest marine influence. This is also supported by palynological evidence from the Nordkapp Basin core, where fresh-to brackish-water algae were documented in the Carnian interval (Hochuli and Vigran, 2010). The tidal influence in the Triassic channels is interpreted to reflect a shallow-gradient delta plain, similar to that described from onshore Svalbard (Knarud, 1980) and from clinoform studies in the Barents Sea (Anell et al., 2014).
4) Little petrographic evidence of significant physical sediment reworking is found in the studied channels. The presence of unstable lithic rock fragments would also suggest dumping of sediments without significant physical reworking. Evidence of detrital grain dissolution is found, but this is more likely related to post-depositional groundwater leaching.

A statistical study of chlorite coatings from a wide range of subsurface examples conducted by Dowey et al. (2012) concluded that prediction of porosity-preserving chlorite coatings must be related to hinterland geology, soil development and river systems. Based on results from the present study, we claim that an understanding the physical process behind grain coating emplacement, and its link to depositional environments and climate conditions that facilitate such processes, are of equal importance for reservoir quality prediction in hydrocarbon plays containing chlorite coatings. Laboratory studies that investigate the physical mechanisms facilitating grain coating emplacement in sediment of various composition and textures is strongly advised.

5.3. Meteoric leaching

Although we have characterized the Middle – Late Triassic channel deposits in this study as physically mature, feldspathic sandstones are considered chemically immature and would be prone to post-depositional chemical alteration by meteoric leaching. Evidence of framework grain dissolution is found in almost all studied samples, but the leaching intensity is generally low and varies between the channels. On average, 3–7% secondary porosity was preserved in the Snadd Formation channels, as opposed to 1% in the Kobbe Formation channel. Feldspathic and metamorphic rock fragments and micas are the most commonly leached framework grains, and dissolution of minerals such as albite, microcline and muscovite result in precipitation of pore-filling authigenic kaolinite. Metamorphic aggregate grains and biotite may have precipitated iron-bearing clays when dissolved (Fig. 9 a–b and e-f). Despite albite and microcline being abundant components in the lithic rock fragment assembly (Figs. 8 and 9), authigenic kaolinite content varies from 0 to 6% in all studied channels (Figs. 4c and 7a-d). As limited kaolinite concentrations cannot be explained by an initial feldspar-poor sediment composition, it is likely the result of restrictions on meteoric leaching.

Consistently low kaolinite concentrations, regardless of channel age and basin location, suggest a temporally stable, regional factor limiting the feldspar dissolution in the basin. Arid and warm climatic conditions are interpreted for the Boreal realm during most parts of the Middle – Late Triassic (Preto et al., 2010; Decou et al., 2017), although periods of increased humidity have been documented (Hochuli and Vigran, 2010; Ogg, 2015; Mueller et al., 2016). The most renown humid interval, the Carnian Pluvial Event (CPE), was assigned to an early Carnian (Julian 1) age in the Boreal region by Mueller et al. (2016) and corresponds to an abrupt short-term sea level increase in the global eustatic sea level curve after Haq et al. (1987) (Fig. 12). The early Carnian channels on the Bjarmeland Platform and the Nordkapp Basin may have been deposited during this climatic phase, but this correlation remains speculative due to inexact dating of the core intervals. Leaching capacity of meteoric water requires gravitational potential, as defined by the elevation above sea level (Bjørlykke, 1993). During marine inundations on the shelf, the gravitational potential is zero and meteoric leaching would stagnate. High sea level coupled with a flat platform gradient could thus explain the limited authigenic kaolinite concentrations (0–3%) in the early Carnian channels. Temporal variations in sea level and climate might explain slight variations in leaching intensity and clay mineralogy between the studied channels, but the overall trend during the Middle – Late Triassic points toward limited chemical weathering and a dominance of mechanical weathering in the basin.

Increased sediment supply from the Ural mountain range could reduce the sediment residence time in the leaching zone. As connate pore water becomes oversaturated with respect to dissolved minerals, efficient replacement of meteoric water is required for leaching to proceed. Weathering rates of K-feldspar and albite at surface temperatures are 520.000 and 190.000 years/mm respectively (Busenberg and Clemency, 1976; Chou and Wollast, 1985), and a stable supply of undersaturated meteoric water over long periods is required before significant leaching of feldspathic sediment is possible. The mineralogy of the investigated channels rather indicates rapid subsidence and burial of the sediment, and thereby favoring preservation of albite and K-feldspar.

Aquifer (channel) permeability may also constrain groundwater leaching capacity by affecting the water flux through the sediment (Bjørlykke, 1993). High concentrations of allogenic matrix in the intergranular volume, as documented in the tidally influenced Kobbe Formation channel, reduce the channel permeability and consequently the leaching capacity. Finer grain sizes in the Anisian channel result in smaller pore neck diameters, and thereby imprisoning infiltrated clay particles and reduce the channel permeability. Variations in leaching intensity could thus relate to an uneven distribution of allogenic clay matrix and varying grain sizes in tidally influenced and fluvial-dominated channels.

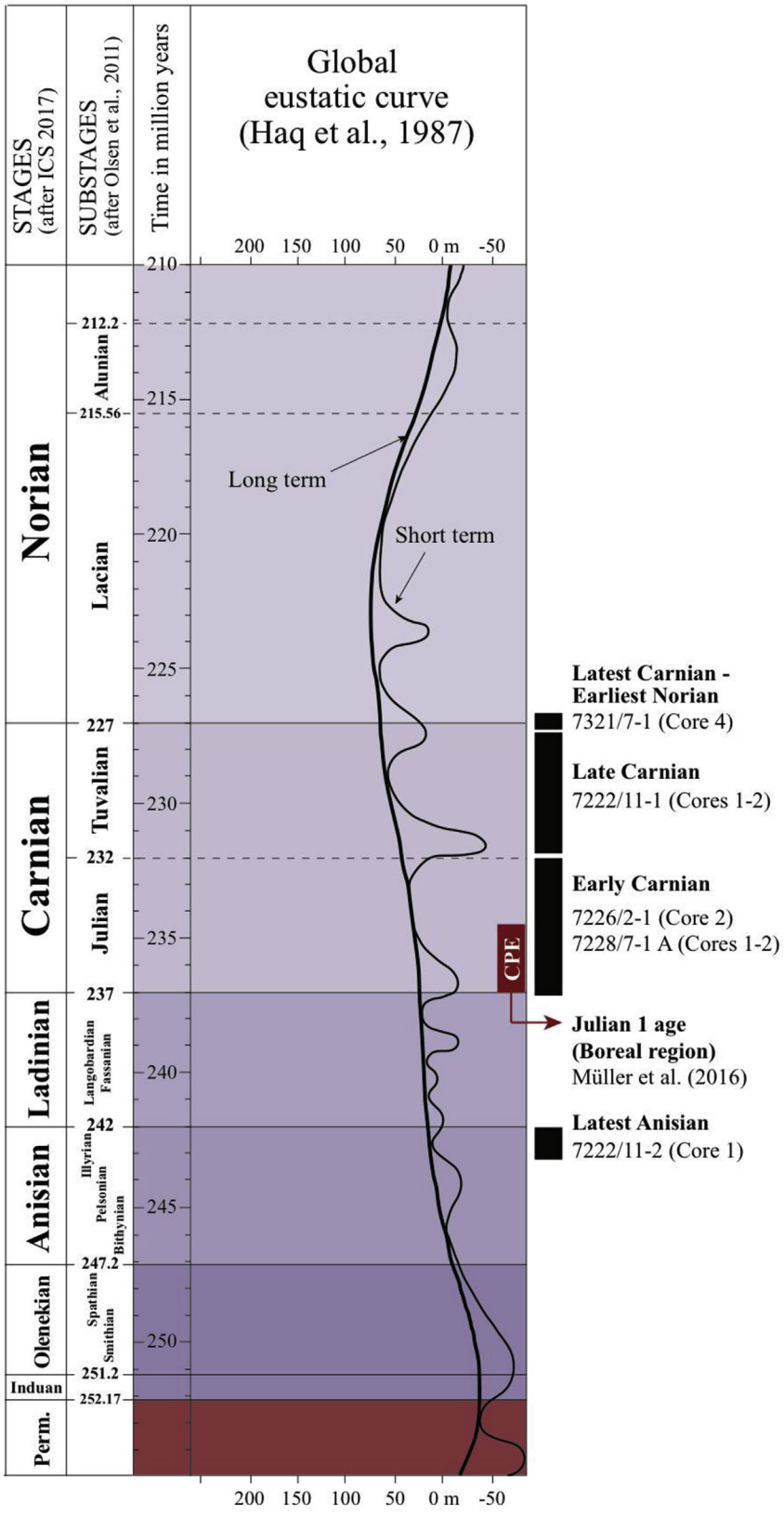

Fig. 12. Long-term and short-term global eustatic sea level curves for the Triassic, modified after Haq et al. (1987). Stage boundaries were retrieved from ICS's chronostratigraphic chart (2017), while substage boundaries were obtained from www.stratigraphy.org. The Carnian Pluvial Event (CPE) in the Boreal region was assigned to a Julian 1 age by Mueller et al. (2016), indicated by the red column. Relative age of core intervals (black columns) were obtained from stratigraphic correlations after Klausen et al. (2015) and palynological records after Hochuli and Vigran (2010). (For interpretation of the references to color in this figure legend, the reader is referred to the Web version of this article.)

5.4. Palaeotemperatures indicated from clay mineralogy

Crystallization temperatures of authigenic cements were used to infer temperature ranges and associated burial depths of the studied cores, by using the present-day average geothermal gradient of 31 °C/km for the southwestern Barents Sea (Smelror et al., 2009). As quartz nucleation initiates around 65–70 °C, the presence of quartz overgrowths indicates a minimum burial depth of approximately 2 km for all the studied channels. Chloritic cements are interpreted as diagenetic overprints concealing the identity of an amorphous precursor clay

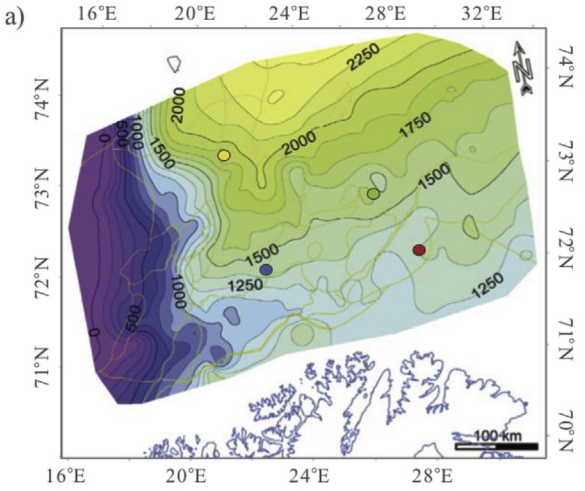

Modified from arithmetic average net exhumation map after Baig et al. (2016).

Well	Estimated net uplift [m]	Calculated maximum burial depth of core interval [m TVD]	Maximum burial temperature [°C]*
● 7222/11-1	1450	2228 - 2250	70
□ 7222/11-2		3556 - 3574	110
● 7228/7-1 A	1375	3434 - 3479	108
● 7226/2-1	1550	2915 - 2967	92
● 7321/7-1	1700	4086 - 4088	127

* Calculated using a geothermal gradient of 31°C/km.

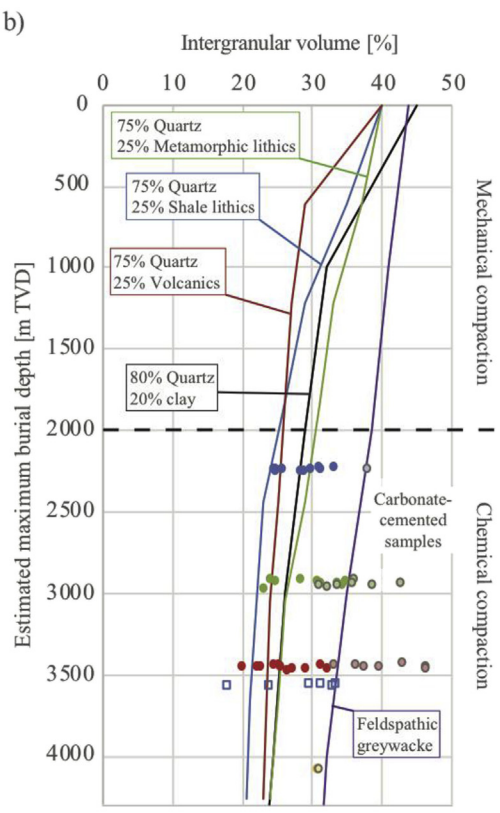

Fig. 13. a) Arithmetic average net exhumation map after Baig et al. (2016), with well locations indicated in colored dots. Calculated maximum burial estimates for cored intervals and associated maximum temperatures calculated from the present-day geothermal gradient in the southwestern Barents Sea (Smelror et al., 2009) are presented in the table below. b) Estimated maximum burial depths versus point-counted IGV from the studied Snadd and Kobbe formations (legend same as listed in table), compared to published experimental compaction curves for various lithologies (Pittman and Larese, 1991; Chuhan et al., 2003; Fawad et al., 2011). Carbonate-cemented samples are indicated with dark circles. Although buried into the chemical compaction regime, the IGV appears to stabilize around 20–30% due to chlorite coatings.

material. Aagaard et al. (2000) found that authigenic chlorite crystals form from iron-rich precursor clays at around 90 °C, adjusting the minimum burial estimate for the investigated channels to 2.9 km. Upper palaeotemperature limits are difficult to estimate using clay mineralogy, but can be inferred from the kaolinite - illite transformation, which occurs at temperatures exceeding 120 °C (Lanson et al., 2002). The presence of vermicular kaolinite and lack of fibrous illite crystals in the studied channels would suggest that the maximum temperature did not exceed 120 °C in any of the investigated channels, yielding a maximum burial depth of 3.8 km.

5.5. Mechanical compaction

Following the arithmetic average net exhumation map after Baig et al. (2016), maximum burial depths differ significantly according to well location (Fig. 13a). Maximal burial depths of the cored intervals, calculated from the exhumation map, were plotted against point counted IGV and compared to experimental compaction curves for various lithologies (Fig. 13b): Well-sorted sands containing 25% metamorphic, sedimentary or volcanic lithics were obtained from Pittman and Larese (1991), a medium-grained quartzite with 20% clay from Chuhan et al. (2003), and feldspathic greywacke after Fawad et al. (2011). Mismatch between natural sandstones and experimental sands is likely related to varying matrix content, which has significant effect on mechanical compaction of sandstones.

Clay mineralogy suggests all studied samples were buried into the chemical compaction regime. However, as extensive quartz overgrowths are absent, chlorite coatings appear to be efficient in inhibiting quartz cement from nucleating on the grain surfaces. The intergranular volume in non-calcite cemented samples appears to stabilize around 20–30% after 2 km burial, suggesting that less than 3% quartz cement is needed to stabilize the grain framework and counteract further mechanical compaction (Fig. 13b). Formation of quartz overgrowths in the studied sandstones thus appear to have a slightly positive influence on reservoir quality as the grain framework become more resistant to mechanical compaction.

Grain contacts reflect the stress level inflicted on the grain framework (Santin et al., 2009) and the sediment response to mechanical stress is linked to mineralogy and textural composition (Fawad et al., 2011). Higher concentrations of lithic aggregate grains with ductile deformation response, e.g. metasediments, volcanic and granitic lithics and sedimentary mudrocks, affect the compressibility of the sandstone (Pittman and Larese, 1991). These grains will likely deform more easily than monocrystalline mineral grains. Ductile framework grain deformation reduces the intergranular volume during mechanical compaction but inhibit grain fracturing and onset of quartz cementation on uncoated surfaces at burial temperatures exceeding 70 °C. Long grain contact dominance in samples from the Nordkapp Basin reflects the high amounts of lithic aggregate grains characterizing this channel (Fig. 7f). Higher relative quartz content in the Bjarmeland Platform

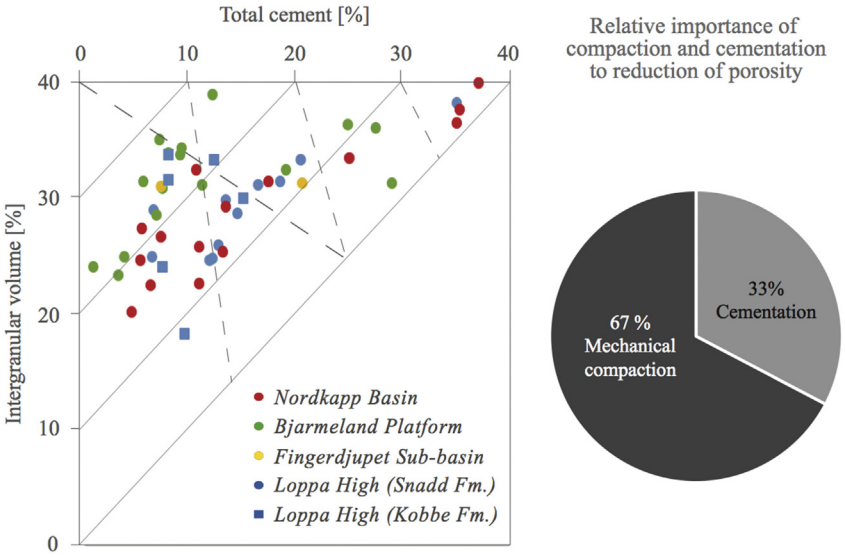

Fig. 14. Intergranular volume plotted versus total cement for the studied samples (modified after Houseknecht, 1987; Ehrenberg, 1989). The dashed line represents a set of points where equal amounts of original porosity (assumed 40%) have been lost to mechanical compaction and cementation. Apart from the calcite-cemented samples plotting in the upper right corner of the diagram, an indisputable abundance of samples has lost their initial intergranular porosity to mechanical compaction, as presented in the pie chart to the right.

channel (Fig. 11) results in a dominance of tangential grain contacts and higher resistance to mechanical compaction, which might explain slightly higher IGV and reservoir quality in this channel (Fig. 7e). The late Carnian channel on the Loppa High has similar mineralogical composition as the channel from the Nordkapp Basin, but the dominance of tangential grain contacts indicates less mechanical compaction in this channel, possibly related to the tectonic evolution of the Loppa High. This is reflected in the reservoir quality, as the best porosity and permeability measurements were located in this channel.

IGV from calcite-cemented samples provide information about intergranular porosities prior to mechanical packing of the sediment. Depending on the amount of matrix material, the initial porosity might have been around 40–45% immediately after deposition. If so, 20% of the intergranular volume has been lost to mechanical compaction in the studied channels. As the mechanical compaction appears to be the main porosity-reducing agent in these sandstones (Fig. 14), future reservoir quality assessments of Middle – Late Triassic channels should include the use of experimental compaction curves for lithologies that are comparable to the Uralian-sourced, feldspathic sandstones.

5.6. Predicting reservoir quality in Middle – Late Triassic channels

5.6.1. Porosity prediction

Intergranular volumes attest to a potential for preserving primary porosity in Anisian and Carnian channels investigated in this study. This is linked to fine grain sizes and precipitation of up to 3% quartz overgrowth, that likely contribute to mechanical strengthening of the grain framework prior to significant burial. Although estimated maximum burial temperatures are above the quartz nucleation threshold, the limited distribution of quartz overgrowth indicates that chlorite coatings efficiently inhibit significant chemical compaction. Porosity prediction in Middle – Late Triassic channels in the Barents Sea is therefore possible if temperature histories and initial sediment compositions are known.

Extensive distribution of porosity-preserving chlorite coatings in the investigated channels provides a unique natural laboratory to study mechanical compaction in deeply buried sandstones. Mechanical compaction experiments should be conducted on sand with the same textural and mineralogical composition as Uralian-sourced sandstones, in order to improve maximum burial estimates. Porosity upside potentials and downside risks should be modelled using various amounts of lithic grains of different types and textures, and various amounts of clay. Early calcite-cemented samples contain information about initial textural properties of the sediment at the surface.

5.6.2. Permeability prediction

Although the potential for porosity preservation appears to be approximately the same for the tidally influenced Anisian channel and fluvial-dominated Carnian channels, the fluvial channels show significantly better permeability compared to the tidally influenced channel in this study. Low permeability measurements correspond to high concentrations of allogenic matrix in this study. Very fine grain sizes with narrow pore neck diameters could have facilitated the entrapment of allogenic clay material, as observed in the Anisian channel on the Loppa High. Fine-grained, clay-rich sandstones may be linked to mud-rich delta sequences that likely developed under repeated influence by marine inundation. Subsidence induced accommodation on a low-gradient delta top could only facilitate transport of fine-grained clastic material to the delta front and basin, which left the Anisian channelized deposits fine-grained and heterolithic in composition (Klausen et al., 2017b). Analogous deposits to the upper part of the Snadd Formation from the De Geerdalen Formation on Hopen island show that tidal and fluvial channels have equal size and geometries, but distinct differences in internal heterogeneities and sedimentary structures (Klausen and Mørk, 2014; Lord et al., 2014). At present, the distinction between mud-rich, tidally influenced channels and clean, fluvial-dominated channels can only be resolved through the study of outcrop analogues or in core. Tidally influenced channels are often associated with other tidal deposits (e.g. channels incising into tidal flat deposits) and marine proximity. Thus the influence of marine processes may therefore be inferred by observing the relationship between the location of a channel and its proximity to known shoreface deposits or palaeocoastlines (Lord, pers. comm., 2018). As subsurface seismic data are unable to resolve distinctive depositional features in various channel reservoirs, pre-drill permeability prediction is considered impossible at present.

5.6.3. Predicting chlorite coating occurrence

Chloritic cements detected in the studied channels are interpreted as diagenetic overprints, representing recrystallization products from a

precursor clay material that was incorporated into the sandstone prior or subsequent to deposition. If sourced from the Uralide mountain range, the channels located in the southwestern Barents Sea represent a distal position on the Triassic delta, which explains the fine grain sizes documented in the fluvial facies. Lithic grains are more abundant in samples collected from eastern parts of the Barents Sea (Mørk, 1999), which represents a proximal position relative to the Uralian provenance. It is likely that the physical endurance of polycrystalline lithic rock aggregates (e.g. metamorphic rock fragments and epidote schists) during fluvial transport is significantly lower compared to monocrystalline quartz and feldspars. Disaggregation of lithic grains with iron-bearing minerals (e.g. epidote, biotite and pyroxene) along the transport profile could represent the origin of the precursor clay material. Continuous contribution from disaggregated mud rock fragments eroded from the floodplain also represents an additional source of the suspended clay fraction in the channels. The clay precursor could have been incorporated into coarser clastic bedload within the channel during high-tide, when the tidal current stagnated the fluvial current. In a mud-rich delta system frequently flooded by marine inundation, it is not unlikely that a clay precursor might have been re-transported into the channels via tidal currents and incorporated into the sediment during slack tide.

From this interpretation, it follows that the distribution of precursor clay material in the Middle – Late Triassic channels (and thus recrystallized chlorite coatings) is provenance-controlled. This hypothesis is supported by an abrupt decrease in chlorite concentrations associated with a shift from dominating Uralian zircon age signatures to more pronounced Fennoscandian and Caledonian age signatures (Bergan and Knarud, 1993; Klausen et al., 2017a). Coatings from Jurassic sandstones in the southwestern Barents Sea usually have illitic chemistry and are scarcely distributed compared to the Triassic chlorite coatings (Clark, 2017). We therefore expect the presence of chlorite coatings within large-scale Uralian-sourced Triassic channels in the southwestern Barents Sea.

From their study of the modern Ravenglass Estuary in northwestern England, U.K., Wooldridge et al. (2017) claimed that the distribution of detrital clay-coated grains can be predicted if specific depositional environment, clay fraction percentage and grain size is known. These authors concluded that the most extensive clay coatings, and consequently the best porosity potential, are expected to occur in fine-grained, clay-bearing inner tidal flat facies sands. However, porosity-preservation alone does not yield the best reservoir quality, as demonstrated in the low-permeable, tidally influenced Kobbe Formation channel. Well-developed and efficient chlorite coatings consistently occur in both fluvial and tidal channel systems, independent of grain size, allogenic matrix concentrations, or basin location. This observation indicates that the precursor coating material develops regardless of channel type (fluvial versus tidal) and is rather the product of provenance and repeated marine inundations. The link to depositional facies can only be obtained by identifying the precursor phase in transmission electron microscopy. Physical mechanisms behind the grain coating emplacement process remains elusive without dedicated laboratory and analogue studies.

6. Conclusion

The Anisian Kobbe Formation channel located on the Loppa High represents a disappointing drilling prospect, where the best reservoir quality is characterized as fair. Despite acceptable intergranular volumes and the presence of efficient chlorite coatings, low permeability properties due to high matrix concentrations reduce the reservoir potential in this channel. The Carnian channels investigated in this paper show good reservoir quality, mainly due to the presence of chlorite coatings and intergranular matrix concentrations below 15%. Mineralogical and textural properties, and basin burial and uplift history are interpreted to control the compaction of Anisian and Carnian sandstones in this study. Development of precursor coatings in the fluvial channel facies is considered vital for later inhibition of chemical compaction by quartz cementation.

It is our understanding that porosity in Middle – Late Triassic fluvial sandstone reservoirs is predictable by coupling initial sediment composition and depositional facies with basin burial history. Chlorite coatings are present in all studied samples from the fluvial sandstone facies, indicating a potential for preserving porosity in reservoirs exceeding temperatures of 70 °C. Mechanical compaction is the abundant porosity-reducing agent, and IGV can likely be predicted by using experimental compaction curves for sandstones with similar petrography as Uralian-sourced sandstones. The abundance of fine grain sizes in distal delta positions yields a large number of grain contacts that mechanically strengthen these sandstone reservoirs.

Allogenic matrix concentration is considered unpredictable and represents the major risk factor for reservoir quality in the Middle – Late Triassic petroleum play. Results from this study indicate that pore-filling matrix material above 15% have a negative impact on reservoir permeability. A link between matrix concentration, grain size and channel type was detected. Distinction between the very fine-grained, matrix-rich tidally influenced channels and clean, fluvial-dominated channels is only possible in outcrop analogue and core studies.

Future exploration strategies for Uralian-sourced sandstone reservoirs should target large-scale, seismically resolvable Carnian channels of the Snadd Formation, as the probability of encountering good reservoir quality is higher in these channels compared to underlying formations such as the Kobbe Formation. Future assessments of the Triassic hydrocarbon play in the southwestern Barents Sea should emphasize temperature and uplift history, as these parameters are understudied and remain highly speculative. Constraining uplift and erosion events are critical for determining the maximum burial depths and the time spent at given temperature conditions (Baig et al., 2016). Regional maps displaying maximum burial temperature distributions in the southwestern Barents Sea are necessary inputs for reservoir and seal properties modelling.

Acknowledgements

The first author of this paper is funded by VISTA – a collaborative (6270), basic research program between The Norwegian Academy of Science and Letters, and Statoil. The scientific contributions of Chloé Franca Marcilly (UiO) and Timea Gyneis (UiO) are greatly appreciated. We thank Gareth Lord (Tyr Exploration) and Knut Bjørlykke (UiO) for their efforts in reviewing our manuscript, and follow-up discussions. Beyene Girma Haile (UiO), Tore Klausen (UiB), Christian Eide (UiB) and Ivar Midtkandal (UiO) have contributed to the study by enlightening discussions. Tullow Oil Norge (by Reidar Müller and Richard Olstad) provided data access and a useful discussion forum. Support from the Trias North project group (funded by the Norwegian Research Council (234152)), particularly by Alvar Braathen (UiO), is also acknowledged. Thank you for your time and effort.

Appendixes

Table A.1
Instrumental parameters used for X-ray diffraction analyses at the Department of Geosciences, University of Oslo (2017). *Clay fraction samples.

Instrumental parameter	Value
Lambda	1.5418 (Cu)
Divergence slit	2 mm
Goniometer radius	280 mm
Soller slit 1	2.5 mm
Soller slit 2	2.5 mm
Sample length	5 mm/*2.5 mm
Sigmaster	12
Mustar	45
Exchange capacity	0.36

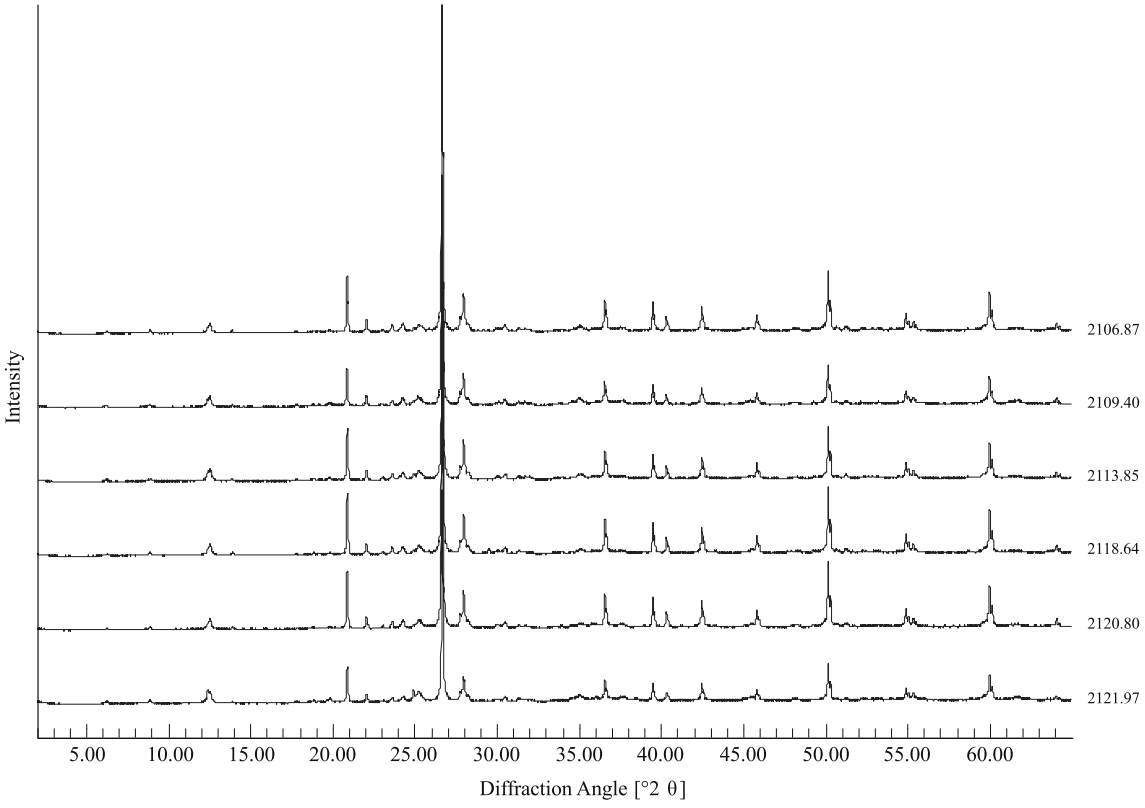

Fig. A.1. Bulk XRD raw data for all channel sandstone samples collected from the Kobbe Formation in well 7222/11–2 (Langlitinden).

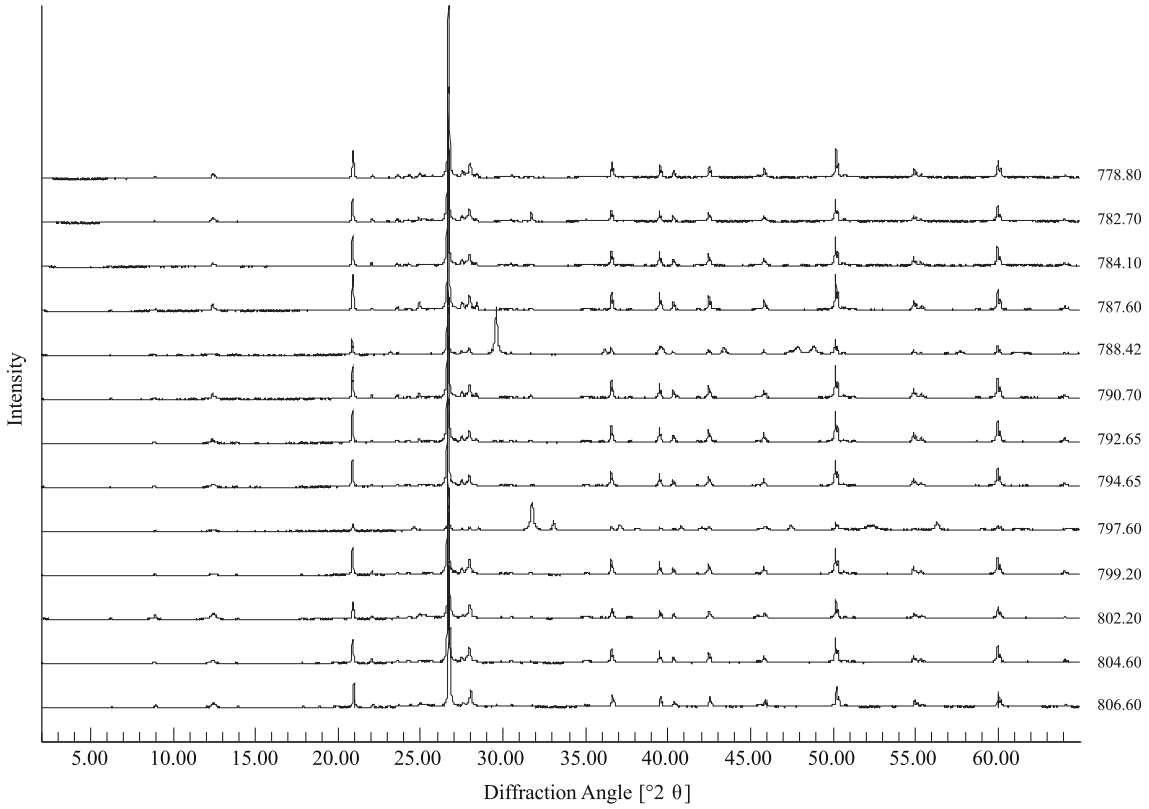

Fig. A.2. Bulk XRD raw data collected from the channel sandstone in Snadd Formation in well 7222/11–1 (Caurus).

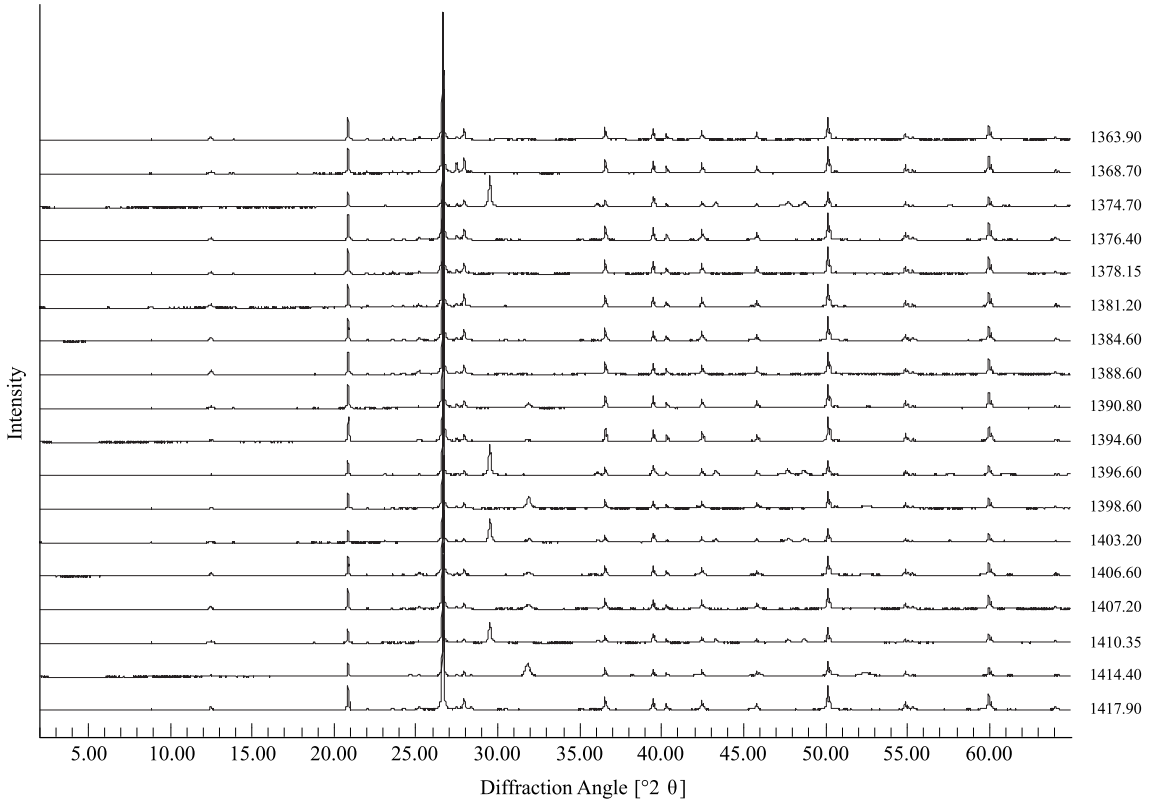

Fig. A.3. Bulk XRD raw data for all channel sandstone samples collected from the Snadd Formation in well 7226/2–1 (Ververis).

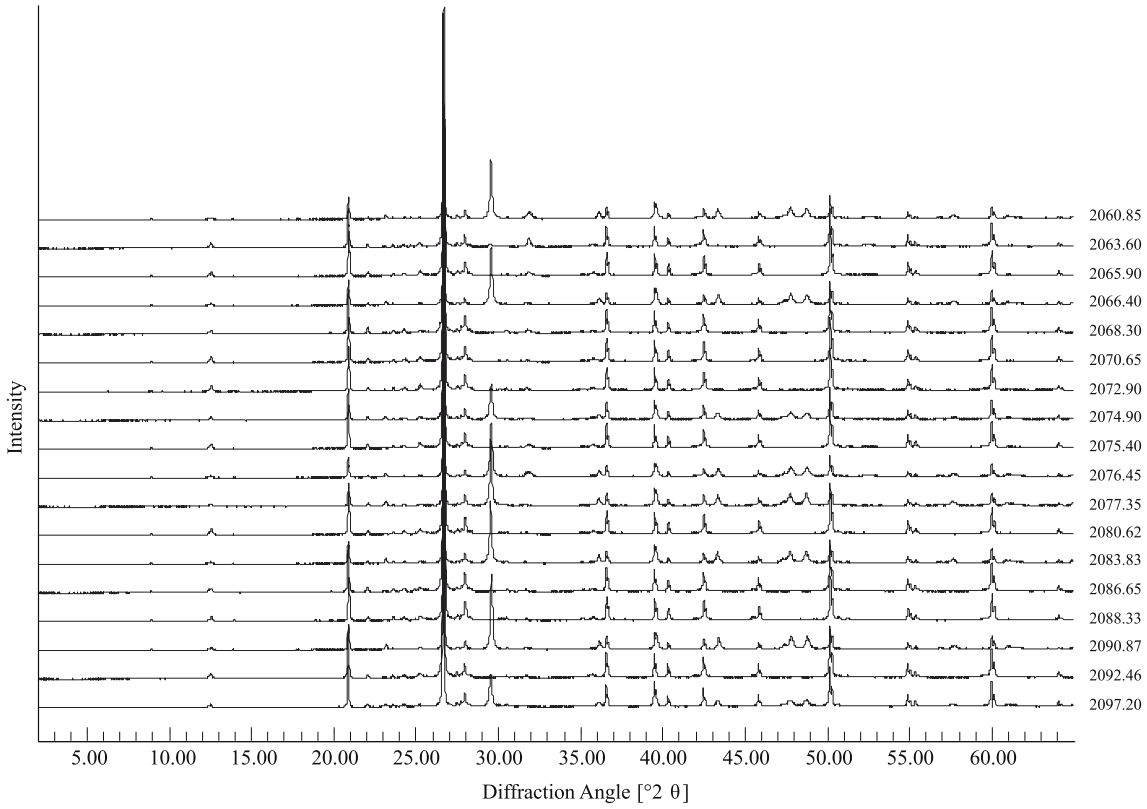

Fig. A.4. Bulk XRD raw data for all channel sandstone samples collected from the Snadd Formation in well 7228/7-1 A (Nordkapp Basin).

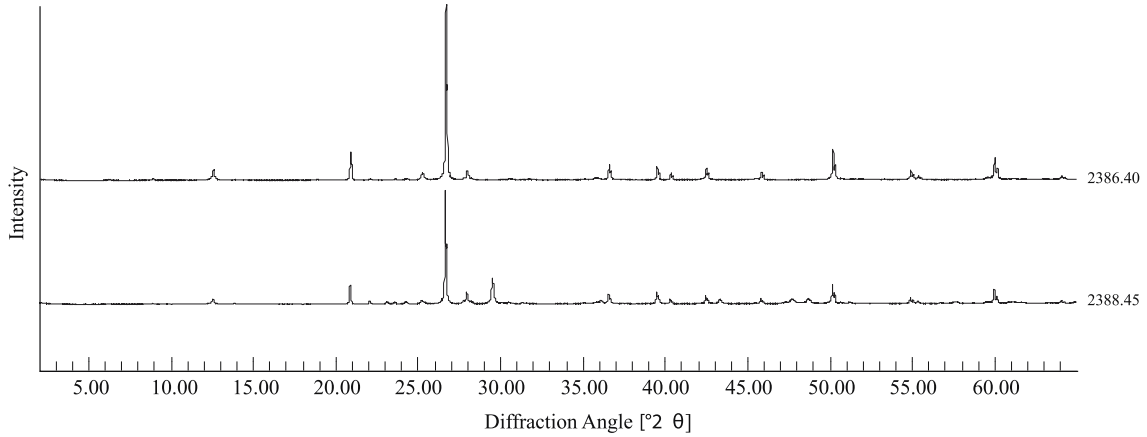

Fig. A.5. Bulk XRD raw data for all channel sandstone samples collected from the Snadd Formation in well 7321/7–1 (Fingerdjupet Sub-basin).

References

Aagaard, P., Jahren, J., Harstad, A., Nilsen, O., Ramm, M., 2000. Formation of grain-coating chlorite in sandstones. Laboratory synthesized vs. natural occurrences. Clay Miner. 35 261–261.

Anell, I., Midtkandal, I., Braathen, A., 2014. Trajectory analysis and inferences on geometric relationships of an Early Triassic prograding clinoform succession on the northern Barents Shelf. Mar. Petrol. Geol. 54, 167–179.

Baig, I., Faleide, J.I., Jahren, J., Mondol, N.H., 2016. Cenozoic exhumation on the southwestern Barents Shelf: estimates and uncertainties constrained from compaction and thermal maturity analyses. Mar. Petrol. Geol. 73, 105–130.

Bergan, M., Knarud, R., 1993. Apparent Changes in Clastic Mineralogy of the Triassic–jurassic Succession, Norwegian Barents Sea: Possible Implications for Palaeodrainage and Subsidence. Norwegian Petroleum Society Special Publications. Elsevier.

Billault, V., Beaufort, D., Baronnet, A., Lacharpagne, J.-C., 2003. A Nanopetrographic and Textural Study of Grain-coating Chlorites in Sandstone Reservoirs. De Gruyter.

Bjørlykke, K., 1993. Fluid flow in sedimentary basins. Sediment. Geol. 86, 137–158.

Bloch, S., Lander, R.H., Bonnell, L., 2002. Anomalously high porosity and permeability in deeply buried sandstone reservoirs: origin and predictability. AAPG Bull. 86, 301–328.

Bue, E.P., Andresen, A., 2014. Constraining depositional models in the Barents Sea region using detrital zircon U–Pb data from Mesozoic sediments in Svalbard. Geol. Soc., London, Special Publications 386, 261–279.

Busenberg, E., Clemency, C.V., 1976. The dissolution kinetics of feldspars at 25 C and 1 atm CO2 partial pressure. Geochem. Cosmochim. Acta 40, 41–49.

Cavanagh, A.J., Di Primio, R., Scheck-Wenderoth, M., Horsfield, B., 2006. Severity and timing of cenozoic exhumation in the southwestern Barents Sea. J. Geol. Soc. 163, 761–774.

Chou, L., Wollast, R., 1985. Steady-state kinetics and dissolution mechanisms of albite. Am. J. Sci. 285, 963–993.

Chuhan, F.A., Kjeldstad, A., Bjørlykke, K., Høeg, K., 2003. Experimental compression of loose sands: relevance to porosity reduction during burial in sedimentary basins. Can. Geotech. J. 40, 995–1011.

Clark, A.F., 2017. Reservoir Characterization of the Fruholmen and Stø Formations in the Hoop Fault Complex, SW Barents Sea.

Decou, A., Andrews, S.D., Alderton, D.H., Morton, A., 2017. Triassic to Early Jurassic climatic trends recorded in the Jameson Land Basin, East Greenland: clay mineralogy,

petrography and heavy mineralogy. Basin Res. 29, 658–673.
Directorate, N.P., 2016. Resource Report 2016. Retrieved from Stavanger, Norway: http://www.npd.no/en/Publications/Resource-Reports.
Dott, R.H., 1964. Wacke, graywacke and matrix–what approach to immature sandstone classification? J. Sediment. Res. 34.
Dowey, P.J., Hodgson, D.M., Worden, R.H., 2012. Pre-requisites, processes, and prediction of chlorite grain coatings in petroleum reservoirs: a review of subsurface examples. Mar. Petrol. Geol. 32, 63–75.
Ehrenberg, S., 1989. Assessing the relative importance of compaction processes and cementation to reduction of porosity in sandstones: discussion; compaction and porosity evolution of Pliocene sandstones, Ventura Basin, California: discussion. AAPG (Am. Assoc. Pet. Geol.) Bull. 73, 1274–1276.
Ehrenberg, S.N., 1993. Preservation of anomalously high porosity in deeply buried sandstones by grain-coating chlorite: examples from the Norwegian continental shelf. AAPG (Am. Assoc. Pet. Geol.) Bull. 77, 1260–1286.
Eide, C.H., Klausen, T.G., Katkov, D., Suslova, A.A., Helland-Hansen, W., 2017. Linking an Early Triassic delta to antecedent topography: source-to-sink study of the south-western Barents Sea margin. Bulletin 130, 263–283.
Enga, J., 2015. Paleosols in the Triassic De Geerdalen and Snadd Formations. NTNU.
Faleide, J.I., Gudlaugsson, S.T., Jacquart, G., 1984. Evolution of the western Barents Sea. Mar. Petrol. Geol. 1 123IN1129IN5137-128IN4136IN8150.
Fawad, M., Mondol, N.H., Jahren, J., Bjørlykke, K., 2011. Mechanical compaction and ultrasonic velocity of sands with different texture and mineralogical composition. Geophys. Prospect. 59, 697–720.
Fleming, E.J., Flowerdew, M.J., Smyth, H.R., Scott, R.A., Morton, A.C., Omma, J.E., Frei, D., Whitehouse, M.J., 2016. Provenance of Triassic sandstones on the southwest Barents Shelf and the implication for sediment dispersal patterns in northwest Pangaea. Mar. Petrol. Geol. 78, 516–535.
Folk, R.L., 1954. The distinction between grain size and mineral composition in sedimentary-rock nomenclature. J. Geol. 62, 344–359.
Folk, R.L., 1980. Petrology of Sedimentary Rocks. Hemphill Publishing Company.
Gabrielsen, R.H., Faerseth, R.B., Jensen, L.N., 1990. Structural Elements of the Norwegian Continental Shelf. Pt. 1. The Barents Sea Region. Norwegian Petroleum Directorate.
Glørstad-Clark, E., Faleide, J.I., Lundschien, B.A., Nystuen, J.P., 2010. Triassic seismic sequence stratigraphy and paleogeography of the western Barents Sea area. Mar. Petrol. Geol. 27, 1448–1475.
Glørstad-Clark, E., Birkeland, E., Nystuen, J., Faleide, J., Midtkandal, I., 2011. Triassic platform-margin deltas in the western Barents Sea. Mar. Petrol. Geol. 28, 1294–1314.
Gould, K., Pe-Piper, G., Piper, D.J., 2010. Relationship of diagenetic chlorite rims to depositional facies in Lower Cretaceous reservoir sandstones of the Scotian Basin. Sedimentology 57, 587–610.
Gudlaugsson, S., Faleide, J., Johansen, S., Breivik, A., 1998. Late palaeozoic structural development of the south-western Barents Sea. Mar. Petrol. Geol. 15, 73–102.
Haile, B.G., Hellevang, H., Aagaard, P., Jahren, J., 2015. Experimental nucleation and growth of smectite and chlorite coatings on clean feldspar and quartz grain surfaces. Mar. Petrol. Geol. 68, 664–674.
Haile, B.G., Klausen, T.G., Czarniecka, U., Xi, K., Jahren, J., Hellevang, H., 2017. How are diagenesis and reservoir quality linked to depositional facies? A deltaic succession, Edgeøya, Svalbard. Mar. Petrol. Geol. 92, 519–546.
Haq, B.U., Hardenbol, J., Vail, P.R., 1987. Chronology of fluctuating sea levels since the Triassic. Science 235, 1156–1167.
Haugen, T., 2016. A Sedimentological Study of the De Geerdalen Formation with Focus on the Isfjorden Member and Palaeosols. NTNU.
Henriksen, E., Ryseth, A., Larssen, G., Heide, T., Rønning, K., Sollid, K., Stoupakova, A., 2011. Tectonostratigraphy of the greater Barents Sea: implications for petroleum systems. Geol. Soc., London, Memoirs 35, 163–195.
Hochuli, P.A., Vigran, J.O., 2010. Climate variations in the boreal triassic—inferred from palynological records from the Barents Sea. Palaeogeogr. Palaeoclimatol. Palaeoecol. 290, 20–42.
Houseknecht, D.W., 1987. Assessing the relative importance of compaction processes and cementation to reduction of porosity in sandstones. AAPG Bull. 71, 633–642.
Høy, T., Lundschien, B., 2011. Triassic deltaic sequences in the northern Barents Sea. Geological Society, London, Memoirs 35, 249–260.
Klausen, T., Mørk, A., 2014. The upper triassic paralic deposits of the De Geerdalen Formation on hopen: outcrop analog to the subsurface Snadd formation in the Barents SeaThe De Geerdalen Formation on hopen. AAPG (Am. Assoc. Pet. Geol.) Bull. 98, 1911–1941.
Klausen, T.G., Ryseth, A.E., Helland-Hansen, W., Gawthorpe, R., Laursen, I., 2014. Spatial and temporal changes in geometries of fluvial channel bodies from the Triassic Snadd Formation of offshore Norway. J. Sediment. Res. 84, 567–585.
Klausen, T.G., Ryseth, A.E., Helland-Hansen, W., Gawthorpe, R., Laursen, I., 2015. Regional development and sequence stratigraphy of the middle to late triassic Snadd Formation, Norwegian Barents Sea. Mar. Petrol. Geol. 62, 102–122.
Klausen, T.G., Müller, R., Slama, J., Helland-Hansen, W., 2017a. Evidence for late triassic provenance areas and early jurassic sediment supply turnover in the Barents Sea basin of northern pangea. Lithosphere 9, 14–28.
Klausen, T.G., Torland, J.A., Eide, C.H., Alaei, B., Olaussen, S., Chiarella, D., 2017b. Clinoform development and topset evolution in a mud-rich delta–the middle triassic Kobbe formation, Norwegian Barents Sea. Sedimentology 65 (4), 1132–1169.
Knarud, R., 1980. En Sedimentologisk Og Diagenetisk Undersøkelse Av Kapp Toscana Formasjonens Sedimenter På Svalbard. (A Sedimentological and Diagenetic Study of the Sediments of the Kapp Toscana Formation in Svalbard). University of Oslo.
Lanson, B., Beaufort, D., Berger, G., Bauer, A., Cassagnabere, A., Meunier, A., 2002. Authigenic kaolin and illitic minerals during burial diagenesis of sandstones: a review. Clay Miner. 37, 1–22.
Lord, G.S., Solvi, K.H., Klausen, T.G., Mørk, A., 2014. Triassic channel bodies on Hopen, Svalbard: their facies, stratigraphical significance and spatial distribution. Norweg. Petrol. Dir. Bull. 11, 41–59.
Lundschien, B.A., Høy, T., Mørk, A., 2014. Triassic hydrocarbon potential in the Northern Barents Sea; integrating Svalbard and stratigraphic core data. Norweg. Petrol. Dir. Bull. 11, 3–20.
Mangerud, G., Rømuld, A., 1991. Spathian-anisian (triassic) palynology at the svalis dome, southwestern Barents Sea. Rev. Palaeobot. Palynol. 70, 199–216.
Matlack, K.S., Houseknecht, D.W., Applin, K.R., 1989. Emplacement of clay into sand by infiltration. J. Sediment. Res. 59.
Mørk, M.B.E., 1999. Compositional variations and provenance of triassic sandstones from the Barents shelf. J. Sediment. Res. 69, 690–710.
Mørk, A., Elvebakk, G., Forsberg, A.W., Vigran, J.O., Weitschat, W., 1999. The type section of the Vikinghogda Formation: a new Lower Triassic unit in central and eastern Svalbard. Polar Res. 18, 51–82.
Mueller, S., Hounslow, M.W., Kürschner, W.M., 2016. Integrated stratigraphy and palaeoclimate history of the carnian pluvial event in the boreal realm; new data from the upper triassic kapp toscana group in central spitsbergen (Norway). J. Geol. Soc. 173, 186–202.
Ogg, J.G., 2015. The mysterious mid-Carnian “wet intermezzo” global event. J. Earth Sci. 26, 181–191.
Pittman, E.D., Larese, R.E., 1991. Compaction of lithic sands: experimental results and applications. AAPG (Am. Assoc. Pet. Geol.) Bull. 75.
Preto, N., Kustatscher, E., Wignall, P.B., 2010. Triassic climates—state of the art and perspectives. Palaeogeogr. Palaeoclimatol. Palaeoecol. 290, 1–10.
Riis, F., Lundschien, B.A., Høy, T., Mørk, A., Mørk, M.B.E., 2008. Evolution of the triassic shelf in the northern Barents Sea region. Polar Res. 27, 318–338.
Ronnevik, H., Beskow, B., Jacobsen, H.P., 1982. Structural and Stratigraphic Evolution of the Barents Sea.
Rønnevik, H., Beskow, B., Jacobsen, H.P., 1982. Structural and Stratigraphic Evolution of the Barents Sea.
Ryan, P., Reynolds, R., 1996. The origin and diagenesis of grain-coating serpentine-chlorite in Tuscaloosa Formation sandstone, US Gulf Coast. Am. Mineral. 81, 213–225.
Santin, C.E., Abel, M., Goldberg, K., De Ros, L.F., June, 2009. Automatic detection of the degree of compaction in reservoir rocks based on visual knowledge. In: Poster Presentation at AAPG Annual Convention and Exhibition, Denver, Colorado, pp. 7–10.
Smelror, M., Petrov, O., Larssen, G.B., Werner, S., 2009. Geological History of the Barents Sea. Geological Survey of Norway, Trondheim.
Stensland, H., 2012. Sedimentology and Diagenesis of the Triassic Snadd Formation in the Barents Sea. Institutt for geologi og bergteknikk.
Tissot, B.P., Welte, D.H., 1984. From Kerogen to Petroleum. Petroleum Formation and Occurrence. Springer.
Vigran, J.O., Mangerud, G., Mørk, A., Worsley, D., Hochuli, P.A., 2014. Palynology and geology of the triassic succession of svalbard and the Barents Sea. Geol. Surv. Nor. Special Publ. 14, 277.
Walderhaug, O., 1996. Kinetic modeling of quartz cementation and porosity loss in deeply buried sandstone reservoirs. AAPG Bull. 80, 731–745.
Woodland, B.G., Stenstrom, R.C., 1979. The Occurrence and Origin of Siderite Concretions in the Francis Creek Shale (Pennsylvanian) of Northeastern Illinois. Mazon Creek Fossils. Elsevier.
Wooldridge, L.J., Worden, R.H., Griffiths, J., Utley, J.E., 2017. Clay-coated sand grains in petroleum reservoirs: understanding their distribution via a modern analogue. J. Sediment. Res. 87, 338–352.
Worsley, D., 2008. The post-Caledonian development of Svalbard and the western Barents Sea. Polar Res. 27, 298–317.
Ziegler, A.M., Parrish, J.M., Jiping, Y., Gyllenhaal, E.D., Rowley, D.B., Parrish, J.T., Shangyou, N., Bekker, A., Hulver, M.L., 1994. Early Mesozoic Phytogeography and Climate. Palaeoclimates and their Modelling. Springer.